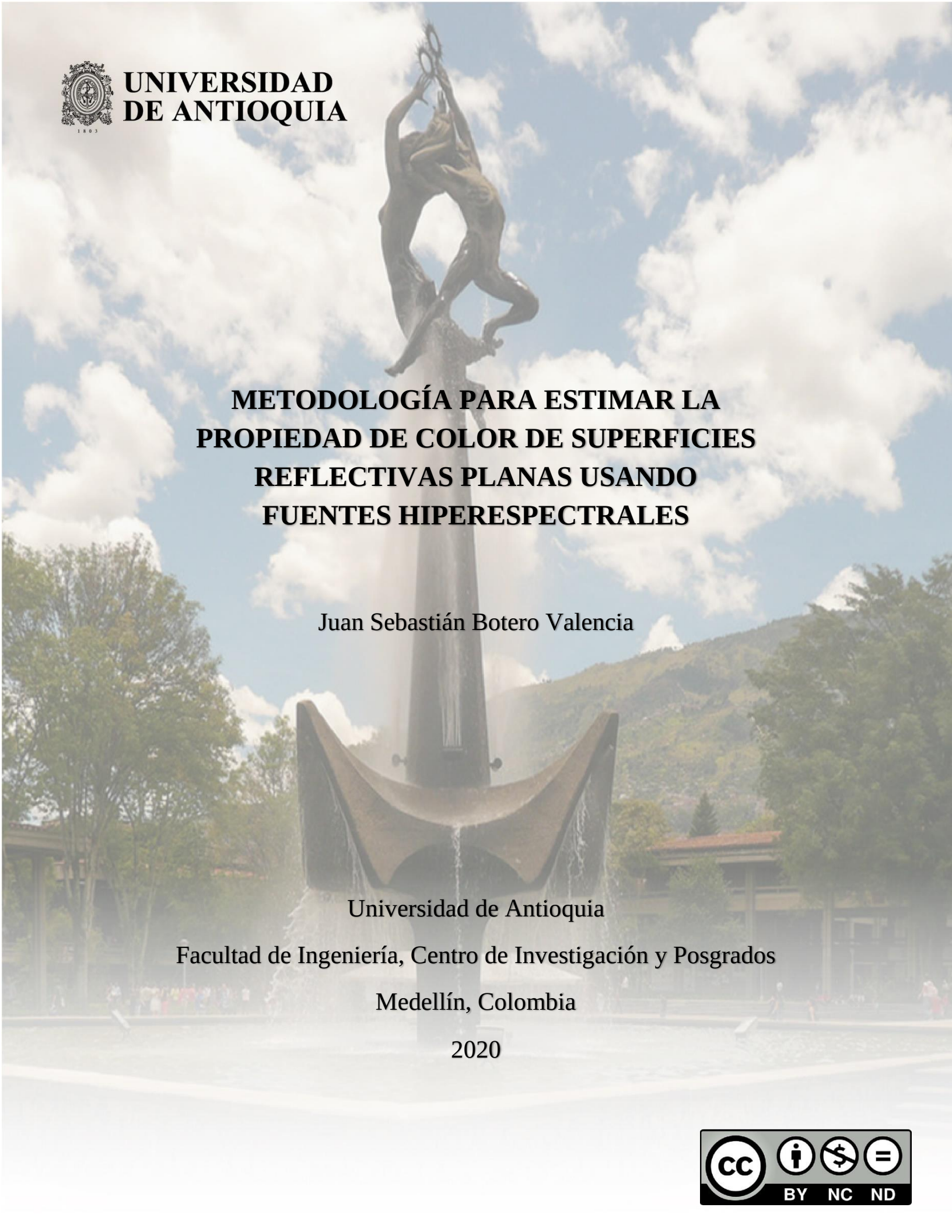

UNIVERSIDAD DE ANTIOQUIA

METODOLOGÍA PARA ESTIMAR LA PROPIEDAD DE COLOR DE SUPERFICIES REFLECTIVAS PLANAS USANDO FUENTES HIPERESPECTRALES

Juan Sebastián Botero Valencia

Universidad de Antioquia

Facultad de Ingeniería, Centro de Investigación y Posgrados

Medellín, Colombia

2020

Metodología para estimar la propiedad de color de superficies reflectivas planas usando fuentes hiperespectrales

Juan Sebastián Botero Valencia

Tesis de investigación presentada como requisito parcial para optar al título de:
Doctor en Ingeniería Electrónica

Asesores:
PhD Jesús Francisco Vargas Bonilla
PhD Francisco Eugenio López Giraldo

Línea de Investigación:
Procesamiento Digital de Señales
Grupo de Investigación:
Sistemas Embebidos e Inteligencia Computacional - SISTEMIC

Universidad de Antioquia
Facultad de Ingeniería, Centro Investigación y Posgrados
Medellín, Colombia
2020

ACKNOWLEDGEMENT

I wish to thank the supervisors of this thesis PhD Jeśus Francisco Vargas Bonilla and PhD Francisco Eugenio López Giraldo for the guidance and cooperation during this time; my parents and siblings for their unconditional support, their patience and their interest in my academic development. And finally, I want to thank the University of Antioquia and especially the Doctoral Scholarship Fund for the support and great opportunity they gave me.

ABSTRACT

Color is a property directly related to light and is dependent on electromagnetic waves in the visible spectrum that are reflected, absorbed or emitted (luminescence) by objects. In non-luminescent Lambertian surfaces, the color is a property that depends directly on the reflectance function and therefore its estimation is essential for measurement. At present there is equipment or systems that allow estimating the color in industrial applications. Most, however, it is costly equipment that is fitted to standardized lighting sources (to generalize), requires strictly controlled measurement conditions, or is only making point measurements on the surface. This doctoral thesis presents the development of a methodology and a functional model that operates under controlled lighting conditions, but which is robust to estimated external perturbations. The model allows to measure color properties on a flat surface from the estimated reflectance values and can be used in the XYZ color space with standardized light sources or representations derived from other sources. Indeed, it was necessary to develop characterization models of the spectral response of photodetectors; on one side, to know the gain at different wavelengths and on the other side, to detect defects and uniformity of the surface response in two-dimensional arrays (chambers). It was also necessary to design and characterize a 23-band LED illumination system to obtain an estimate of the surface reflectance function, and a model that would allow, using low-cost photodetectors, finding indicators to detect and correct external disturbances, which may be present on the measuring surface. Finally, a model was developed that integrates different subsystems using a Multi Layer Perceptron to calculate the color in the XYZ space on the test surface with an error lower than 1%.

Keywords: Color measurement, flat surfaces, Lambertian surfaces, hyperspectral source, reflectance, XYZ space.

RESUMEN

El color es una propiedad directamente relacionada con la luz y es dependiente de las ondas electromagnéticas reflejadas, absorbidas o emitidas (luminiscencia) por los objetos en el espectro visible. En superficies Lambertianas no luminiscentes, el color es una propiedad que depende directamente de la función de reflectancia de la misma y por tanto su estimación es fundamental para la medición. En la actualidad existen equipos o sistemas que permiten estimar el color en aplicaciones industriales, sin embargo, en su gran mayoría son equipos costosos que están ajustados a fuentes de iluminación estandarizadas (buscando generalizar), que requieren estrictas condiciones controladas de medición o solo realizan mediciones puntuales en la superficie. En este trabajo se presenta el desarrollo de una metodología y un modelo funcional que opera bajo condiciones de iluminación controlada, pero que es robusto a perturbaciones externas estimadas y que permite medir propiedades del color sobre una superficie plana a partir de los valores de reflectancia estimados y que pueda llevarse al espacio de color XYZ con las fuentes de iluminación estandarizadas o a representaciones derivadas con otros fuentes. Para esto fue necesario desarrollar modelos de caracterización de la respuesta espectral de fotodetectores, de un lado para conocer la ganancia a diferentes longitudes de onda y de otro lado para detectar en los arreglos bidimensionales (cámaras) los defectos y la uniformidad de respuesta de la superficie. También fue necesario diseñar y caracterizar un sistema de iluminación LED con 23 bandas que permite obtener una estimación de la función de reflectancia de la superficie y un modelo que permitiera usando fotodetectores de bajo costo derivar indicadores sobre la luz para detectar y corregir las perturbaciones externas que se puedan presentar en la superficie de medición. Finalmente se desarrolló un modelo que integra los diferentes subsistemas usando una Multi Layer Perceptron para calcular el color en el espacio XYZ en la superficie de prueba con un error inferior al 1%.

Palabras Clave: Medición de color, Superficie plana, superficie Lambertiana, fuente hiperespectral, reflectancia, espacio XYZ.

CONTENTS

List of Figures

List of Tables

1

INTRODUCTION

Contents

1.1. COLOR VISION

Color vision was developed in our species by genetic duplication of the cones [1]. Humans have a trichromatic vision system with the greatest response to wavelengths close to 550 nm, wherein the visible spectrum comprises the wavelengths between 380 nm (violet) and 780 nm (dark red). The response of the human eye is not proportional to the values originally established in the construction of the RGB color space (non-linear), so that it became necessary to develop new measurement methods that corresponded linearly to the response of the standard eye. For this the spaces L, a, b were constructed. The spaces L, a, b (CIE -Commission Internationale de l'éclairage L, a, b and Hunter L, a, b) allow to use a scale that varies linearly with human perception. The measurement equipment is linked to the study of light sources to measure the waves that are reflected in the objects and hence to measure the intensity of the reflected wave. Color is a property directly related to light and is dependent on electromagnetic waves in the visible spectrum that are reflected, absorbed or emitted (luminescence) by objects. In non-luminescent Lambertian surfaces, the color is a property that depends directly on the reflectance function and therefore its estimation is essential for measurement.

Figure 1.1 shows the CIE curves that numerically represent the response of a standard observer. These functions can be seen as the sensitivity of three linear detectors that produce the CIE XYZ tristimulus value. The set of functions is known as the standard of the observer, in "CIE standard colorimetric observer tables" they are defined and currently used as reference.

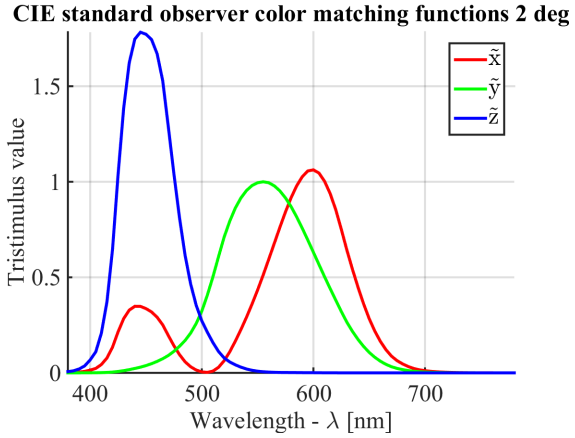

Figure 1.1 CIE 1931 observer

1.2. COLOR SPACE CIE 1931 XYZ

The XYZ color space was developed in 1931 from the data of W. David Wright and John Guild found in 1920, and its derivation is explained in [2]. The XYZ color space is characterized, because the Y channel represents the luminosity, the Z channel the blue color and the X channel represents a mixture between red and green. The CIE XYZ coordinates can be calculated using the Spectral Power Distribution (SPD) of the source (I), using the CIE curves, and knowing the reflectance function of the Surface S. The equations are presented in equation (1.1), where K is a constant to normalize Y to 100.

$$X = K \sum_{\lambda=380}^{780} I(\lambda)\cdot S(\lambda)\cdot \tilde{x}(\lambda); \qquad Y = K \sum_{\lambda=380}^{780} I(\lambda)\cdot S(\lambda)\cdot \tilde{y}(\lambda); \qquad Z = K \sum_{\lambda=380}^{780} I(\lambda)\cdot S(\lambda)\cdot \tilde{z}(\lambda) \tag{1.1}$$

1.3. OBJECTIVES

1.3.1. GENERAL

The general objective of this work was the development of a methodology to measure color in the CIE XYZ color space on a flat surface under controlled conditions, which can be dynamically calibrated.

1.3.2. SPECIFIC

1. Definition of a lighting methodology suitable for performing multiplexing of the visible spectrum.
2. Identification of design conditions in the test environment that allow optimizing the color acquisition.
3. Construction of an estimator with the use of spectroscopy that allows evaluating the lighting conditions in the test environment.
4. Construction of an estimator using spectroscopy to determine the surface reflectance function.
5. Integration of a methodology to measure color on a surface with dynamic calibration, integrating information from illumination and reflectance sources.
6. Comparison between of the performance of the developed methodology and obtained by a Spectroradiometer in the CIE XYZ color space.

1.4. ORGANIZATION OF THE DOCUMENT

1.4.1. CHAPTER 1: INTRODUCTION

This section presents the basic concepts of the XYZ color space, the objectives of the work, the distribution of the chapters and the publications that have been derived from this work. Since each section contains an abstract and an introduction that includes the state of the art of each topic.

1.4.2. CHAPTER 2: CHARACTERIZATION OF PHOTODETECTORS

In this chapter, a model was developed to obtain the response of a low cost RGB photodetector. The methodology consists of obtaining the response of each detector at different wavelengths (41) in the visible spectrum processed by a mechanical monochromator. The monochromator input is a calibrated white light source with response throughout the visible spectrum. The method allows estimating the sensitivity of each of the photodetectors and defining an approximation of the spectral response.

1.4.3. CHAPTER 3: CALIBRATION OF CAMERAS

In this chapter we present an experiment and a calibration model that allows us to detect defective pixels, validate the response of a camera to a specific wavelength, and estimate its sensitivity curve. For this, an experiment was designed to generate monochrome light in 21 different bands in the VIS (visible). With this kind of light the surface of the sensor of the camera was illuminated and at the same time a power meter and a mechanical system that rotates the camera automatically were integrated to improve the experiment. Also a second mechanical system was integrated that subducts or approaches the photodetector so that the received power is always the same regardless of the wavelength. Factors such as attenuation in the optical fiber, or non-uniformity of the spectrum of the input source require this translation.

1.4.4. CHAPTER 4: ESTIMATION OF THE LIGHT INDEX

In this section, a methodology for estimating CRI (Color Render Index) and GAI (Gammut Area Index) using the information provided by low-cost RGB sensors with a Multi Layer Perceptron (MLP) is presented. To validate the effectiveness of the methodology, the estimation error was evaluated for two different commercial sensors (TCS3414CS and ADJDS311) and also the compromise between error and training time. In total, 640 MLP architectures were trained by varying the number of layers, the number of neurons per layer, the activation function and the calculation architecture (CPU vs GPU), which significantly affects training time and is reflected in the estimation error due to the use of the floating point. In addition, as a contribution to this work, a database was built with more than 120 000 combined source spectra (artificial and sun) that will serve as a reference to develop new estimation methods. Finally, the results show the effectiveness of the method to train an MLP with an absolute error of less than 2 to estimate the GAI and the CRI with both sensors.

1.4.5. CHAPTER 5: ESTIMATION OF THE REFLECTANCE CURVE

In this chapter, we present a methodology to estimate the reflectance of a flat surface in the visible spectrum using a low-cost 23-band hyperspectral source built with high power (3 W) LEDs, and a monochrome camera. The design of the structure, the adjustments on the camera and the calibration of the system with a reference target are shown to estimate the reflectance. The effectiveness of the estimation is evaluated with the patches of a Color Checker Passport, where the reflectance for each of the 24 samples is known. The method has an error that varies between 2.15% and 22%, being the worst case the one of the black patch that shows very low reflectance.

1.4.6. CHAPTER 6: MODEL INTEGRATION

In the final chapter, we introduce a model that uses an MLP that estimates the color on a surface in the XYZ space and that is robust to disturbances from external light sources with an error lower than 2%. For this, using the experimental data from chapters 2, 3, 4 and 5, a simulation model was developed to construct an artificial database with 80000 samples of reflective surfaces created from combinations of patches of the Color Checker. Random perturbations have been added to the simulation model for the database sources developed in Chapter 4, so that the trained system does not have to work under optimal control conditions. The 23 reflectance points

(corresponding to the response for each LED of the hyperspectral source) are entered into the trained MLP and the CRI and GAI values of the disturbance are measured with the method developed in Chapter 4 before the estimation process is started. The output of the MLP is the color estimation in the XYZ space. The results show that the error is less than 2% even with external disturbances that can reach up to 20% of the power of the hyperspectral source.

1.5. CONTRIBUTIONS

In the development of this thesis the following works have been published:

1. Botero V., J.-S., López G., F.-E., Vargas B., J.-F. (2015). Classification of artificial light sources and estimation of Color Rendering Index using RGB sensors , K Nearest Neighbor and Radial Basis Function. International Journal on Smart Sensing and Intelligent Systems, 8(3), 1505–1524.
   Retrieved from http://www.s2is.org/Issues/v8/n3/papers/paper5.pdf

2. Botero V., J.-S., Navarro, S.-M., Giraldo, N., Atehortua, L. (2014). Estimation of Photosynthetically Active Radiation (PAR) using a low cost spectrometer. IEEE Latin America Transactions, 12(2), 107–111.
   https://doi.org/10.1109/TLA.2014.6749525

3. Botero V., J.-S., López G., F.-E., Vargas B., J.-F. (2016). Characterization of photodectors using a monochromator and a broadband light source in the XYZ color space. International Journal on Smart Sensing and Intelligent Systems, 9(2), 752–764.
   Retrieved from http://s2is.org/Issues/v9/n2/papers/paper18.pdf

4. Botero V., J.-S., López G., F.-E., Vargas B., J.-F. (2013). Calibration Method for Measuring the Color Rendering Index (CRI) using RGB Sensor. Tecnológicas, EE, 325–338.

5. Botero V., J.-S., López G., F.-E., Vargas B., J.-F. (2013). Calibration method for Correlated Color Temperature (CCT) measurement using RGB color sensors. In Symposium of Signals, Images and Artificial Vision - 2013: STSIVA - 2013 (pp. 1–6). Bogotá: IEEE.
   https://doi.org/10.1109/STSIVA.2013.6644921.

And the following works are submitted:

1. Method of estimation of CRI and GAI with a low cost RGB sensor using Multi Layer Perceptron

2. Calibration method for the wavelength and uniformity of pixel response in photodetector arrays

3. A simple method for estimate reflectance in flat surfaces using a LED array

REFERENCES

[1] F. Lopera R., "Evolución y Cognición," *Revista Neuropsicología, Neuropsiquiatría y Neurociencias*, vol. 6, pp. 27–34, 2004. [Online]. Available: http://neurociencias.udea.edu.co/revista/PDF/REVNEURO{_}vol6{_}num1{_}3.pdf

[2] H. S. Fairman, M. H. Brill, and H. Hemmendinger, "How the CIE 1931 color-matching functions were derived from Wright-Guild data," *Color Research & Application*, vol. 22, no. 1, pp. 11–23, feb 1997.

2

CHARACTERIZATION OF PHOTODECTORS

Contents

2.1. ABSTRACT

Photodetectors are sensors, which respond to the electromagnetic radiation of the spectrum. Their spectral response depends on many factors of the manufacturing process, e.g. the type of diode that is used or, in some cases, the optical elements that are added to limit the response band. In this chapter, we propose an experimental methodology to obtain the spectral response of a photodetector by constructing the characteristic curve using the monochromatic response. For this purpose we use a broadband source as input of the monochromator to vary the wavelength each 10 nm. The characteristic curves of one commercial color sensor were obtained (including the loss) using the output ratio of the monochromator. Via the numerical expression of the response curve, it is possible to model the actual response of the photodetectors to known or simulated spectra of electromagnetic radiation, and thus to generalize photometric measurements. Finally, this newly developed method helps studying the behavior of a photodetector in detail; hence it enables the derivation of photometric measurements from known data or simulations.

2.2. INTRODUCTION

Photodetectors are sensors that convert electromagnetic energy into an electrical signal. Its function is to show a particular spectral region as output. They are almost always made of semiconductors that are responsive to photo-excitation and include optical filters to limit the response region among other methods of manufacture [1, 2]. The visible light is a small segment of the electromagnetic spectrum comprised of wavelengths between 380 nm and 780 nm. Nowadays its research is one of the most important fields worldwide; its influence on our behavior has been widely demonstrated [3–7] and the effect on multiple biological systems such as plants [8, 9] and stem cells [10, 11], or on food quality [12] is studied. The interest in the study of new applications and the difficulty in taking measurements, which occurs in some cases, have sparked interest in novel models to perform experiments, and to develop light control applications more accurately and at a lower cost.

The applications for photodetectors are manifold, the most common are varying photometric measurements [13–15], applications where infrared radiation is used [16–21] and where color measurement is required [22–28], intelligent lighting control [13, 29, 30], the derivation of measures such as CCT (Correlated Color Temperature) [31], the estimation of the CRI (Color Rendering Index) [32] and the determination of power measurements in more particular cases such as PAR (Photosynthetically Active Radiation) [33]. However, the response of low-cost photodetectors is not adjusted to the referred measurements and approximations or transformations are necessary, i.e. calibration models [22, 27, 28] that allow interpreting the output data as a reliable measure. Though, this procedure involves extensive experimental work, which is usually done by taking one part of the sample space with known characteristics that allows obtaining the inverse model of the photodetectors. The inverse model is difficult to generalize, due to the impossibility to determine the full sample space, as in the characterization of light sources [31, 32], where it is not possible to include all possible and purchasable light sources while performing the training of the sensor, taking into account that although the initial process is long, the data of the curve can be used to train systems with other measures. The same effect occurs when color charts or nonstandard light sources are used for calibrating the color sensors. A further problem is that the adaption of inverse models again requires experimental procedure.

In this chapter a model was developed and implemented to obtain the characteristic curve of low-cost photodetectors using a broad-band light source, a monochromator and a high resolution spectrometer. Initially the light passes the monochromator and splits into two beams. One of them goes to the spectrometer to measure the power and the other one goes to the photodetector to assess the value of the output signal. This procedure is repeated varying the output wavelength of the monochromator in steps of 10 nm in the visible region absorption spectrum. For each photodetector 41 points are obtained, and then adjusted to compensate the losses occurring in the optical fiber. The monochromator, as well as the source response, are not completely flat; therefore, the beam is split and measured in the spectrometer. The adjusted data represents the spectral response or the characteristic curve of the sensor. The mathematically expressed characteristic curve allows implementing interpolation models of discrete measures from simulated spectra or from known reflectance functions, as in the case of color palettes. The presented methodology reduces the necessity of experiments and allows constructing multiple models from the same photodetector's curve. The datasets of spectra from light sources and reflectance functions of color charts are widely distributed, which allows turning the sensors into measuring devices based on the simulation. As a result of the proposed methodology, the response curve of the TCS3141CS sensor was obtained. The measurement data of the Macbeth color palette was directly obtained with the sensor and the estimated values were obtained with the curve using methodology. As a result of the comparison an error below 3.6 error was found.

This chapter is organized as follows: In section 2 are described the photodetectors, the light source and the spectrometer used for the calibration. Section 3 explains the experimental methodology and the scheme for obtaining the characteristic curve. Section 4 discusses the implemented model and its features and section 5 the process of interpreting the measurements and the interpolation model is exhibited in detail. And finally, section 6 presents the conclusions and future perspectives of the chapter.

2.3. MATERIALS AND METHODS

2.3.1. BROADBAND LIGHT SOURCE EQ99

The EQ-99 is a Laser-Driven Light Source (LDLS) UV-VIS-NIR manufactured by ENERGETIQ. This broadband source is specially designed for high brightness and high stability. The spectral output ranges from 170 nm to 2100 nm, with a Numerical Aperture (NA) up to 0.47 and a typical bulb life longer than 5000 h. For the model presented in this work it is crucial that the light source shows a flat spectral response. Figure 2.1 shows the spectral response of the LDLS, the advantage of a source like this is to have a power response in the visible spectrum as well as being electronically stabilized.

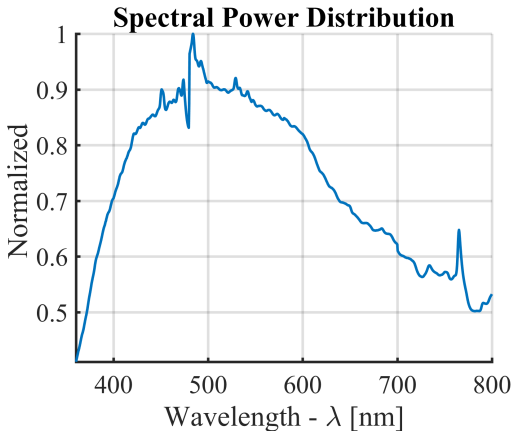

Figure 2.1 Spectral response EQ99

2.3.2. MONOCHROMATOR MINICHROM

Mini-Chrom is a monochromator that uses a dial to select the output wavelength. A screw bar mechanism accurately guides the rotation of a diffraction grating, which positions the selected wavelength at the output. The wavelength is read directly in nanometers (nm) by a four-digit counter in all models. The operating range is 200 nm to 800 nm. SMA connectors will be adapted at the input and output for connecting plastic optical fibers. The advantage of using a monochromator is having a system to control the wavelength with a constant bandwidth which makes it very useful as a reference.

2.3.3. SPECTRUM ANALYZER AQ6373

The AQ6373 is a Spectrum Analyzer that provides an accurate high-speed analysis of the wavelength range between 350 nm and 1200 nm. This OSA is well suited for general purposes. It also allows USB storage, which saves data in flat format for further analysis.

2.3.4. COLOR SENSOR TCS3414CS

TCS3414CS is a color sensor manufactured by Texas Advanced Optoelectronic Solutions (TAOS). It comprises of an 8x2 array of filtered photodiodes, four of them have red filters, four blue, and four green; the remaining four are not filtered. Each of the four sensor channels (Red, Green, Blue, Clear) delivers its output in a format of 16 bits using I2C protocol information at 400 KHz. The gain of the analog converter and the integration time are programmable. The sensor has a synchronization input (SYNC), which allows the precise control of integrated external sources. Table 2.1 shows some important features of TCS3414CS.

Table 2.1 Characteristic TCS3414CS

Characteristic	Value	Units
Sensor	Photodiode	[NA]
Clock frequency	0-400	[KHz]
A/D Resolution	16	[bits]
Channels	R, G, B, clear	[NA]

2.3.5. EXPERIMENT DESCRIPTION

In Figure 2.2 the explanatory diagram of the proposed experiment is presented. Below its parts are described:

1. The system input is a white light source (1) EQ-99 (polychromatic) with UV-VIS-NIR emission.

2. The white light enters a mechanical UV-VIS-NIR monochromator (2) (Mini-Chrom) that selects the desired wavelength. Adjusting the wavelength is carried out manually with a mechanical element at intervals of 10 nm in the visible spectrum (380-780 nm).

3. The output of the monochromator must be demultiplexed (7) into two identical outputs. One of them is led to the spectrometer (6), as a reference value, and the second one to the photodetector (3) to be evaluated, that through a microcontroller (4) transmit the values to a PC (5).

4. The values obtained in the previous stage allow, first, the gain of the photodetector at a certain wavelength and, second, the total VIS-NIR scan (point to point) to reconstruct the spectral response curve of the photodetector.

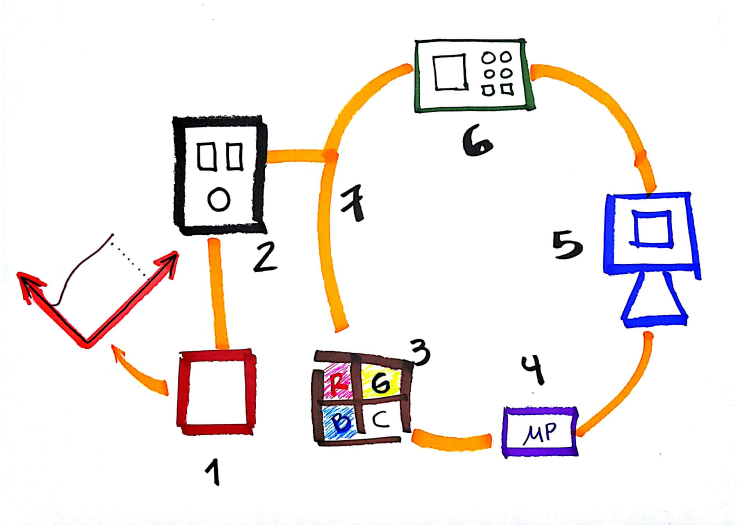

Figure 2.2 Experiment description

2.3.6. COLOR EQUATION

Values in the color space X, Y, Z of a surface can be obtained using the model shown in equation 2.1. Where $E(\lambda)$ represents the source, $P(\lambda)$ the reflectance curve and $\tilde{x}(\lambda)$, $\tilde{y}(\lambda)$ and $\tilde{z}(\lambda)$ the curve of the observer.

$$X = k \sum_{\lambda=380}^{780} E(\lambda) \cdot P(\lambda) \cdot \tilde{x}(\lambda)$$

$$Y = k \sum_{\lambda=380}^{780} E(\lambda) \cdot P(\lambda) \cdot \tilde{y}(\lambda) \tag{2.1}$$

$$Z = k \sum_{\lambda=380}^{780} E(\lambda) \cdot P(\lambda) \cdot \tilde{z}(\lambda)$$

2.3.7. COLOR CHECKER

The color checker is a color palette with 24 samples arranged in 4 rows. The reflectance of the samples are known, allowing to use it as a reference standard. In figure 2.3 the distribution of the colors is shown. With the reflectance information of the Color Checker and given that the source spectrum is known, one can calculate the value of the XYZ space using Equation 2.1.

Figure 2.3 Color checker

2.4. RESULTS AND DISCUSSIONS

2.4.1. SPECTRAL RESPONSE OF THE SENSOR

In principle and using the model described in Figure 2.2 in particular, the spectra are obtained at the exit of the monochromator. Measurements of spectra were taken every 10 nm (in the range 380 to 780 nm) to a total value of 41 spectra, and repeated four times. The spectra are narrow allowing for improved estimation of the response model to be generated. The peak values obtained in this step enable the estimation of the normalized response of the sensor (each channel) to each of the 41 points.

With the normalized monochromator output values, the TCS3414CS sensor response was evaluated. As mentioned, the values obtained in the previous step (peaks) are needed to obtain the gain of each of the photodetectors for each one of the RGB channels. The spectral response curve obtained at the end of the process is presented in Figure 2.4. It corresponds to the one provided by the manufacturer. In total, there are 41 reference points per channel that can be used to perform simulations of the sensor response when they are stimulated with known spectra.

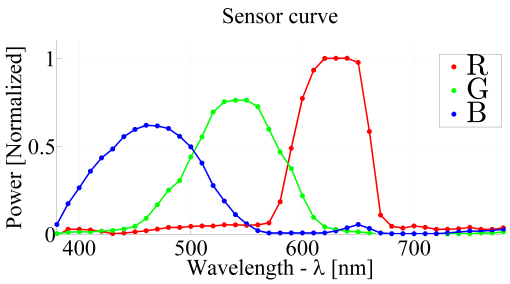

Figure 2.4 Sensor response TCS3414CS

2.4.2. COLOR ESTIMATION

To evaluate the data in the theoretical model, it is necessary to know the spectrum of the light source that will accompany the color sensor for measurement (Figure 2.5), i.e. $E(\lambda)$ in (2.1).

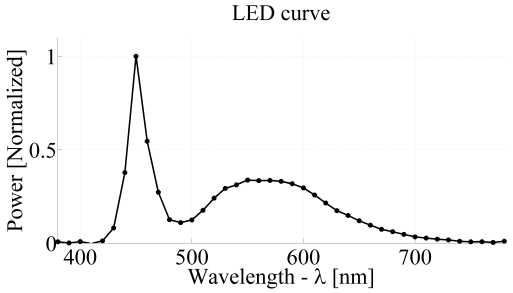

Figure 2.5 SPD White LED

Table 2.2 shows the values from the XYZ measurements using the sensor on the color checker (XM, YM, ZM) and using the response curve found with the proposed methodology (XE, YE, ZE). Finally, in Table 2.2, the estimation error for each channel, and each sample is presented, which is calculated with the absolute difference between the real and estimated value. The highest error value is 0.0036 (the error is normalized) and occurs in white color, the error is low, considering that was used a low cost sensor. The error is expected due to the resolution of the spectral response curve (10 nm), however the experiment demonstrates the effectiveness of the curve to use simulated data and interpolate measures with the sensor.

Table 2.2 XYZ color estimation

Color	XE	XM	YE	YM	ZE	ZM	ER-X	ER-Y	ER-Z
01 Dark Skin	0,136	0,134	0,119	0,120	0,082	0,081	0,000	0,001	0,001
02 Light Skin	0,430	0,427	0,350	0,330	0,258	0,255	0,003	0,020	0,003
03 Blue Sky	0,138	0,134	0,231	0,230	0,302	0,290	0,004	0,001	0,012
04 Foliage	0,111	0,098	0,173	0,160	0,093	0,081	0,013	0,013	0,012
05 Blue Flower	0,220	0,219	0,274	0,280	0,385	0,382	0,000	0,006	0,002
06 Bluish Green	0,219	0,219	0,509	0,491	0,424	0,429	0,000	0,019	0,004
07 Orange	0,467	0,475	0,290	0,280	0,100	0,093	0,008	0,010	0,007
08 Purplish Blue	0,098	0,098	0,164	0,160	0,344	0,336	0,001	0,003	0,007
09 Moderate Red	0,377	0,390	0,164	0,170	0,141	0,151	0,014	0,006	0,009
10 Purple	0,096	0,098	0,082	0,090	0,127	0,127	0,002	0,009	0,000
11 Yellow Green	0,305	0,329	0,495	0,501	0,164	0,185	0,024	0,005	0,021
12 OrangeYellow	0,505	0,524	0,424	0,420	0,119	0,127	0,020	0,003	0,009
13 Blue	0,051	0,049	0,094	0,098	0,246	0,243	0,002	0,004	0,003
14 Green	0,121	0,122	0,285	0,280	0,128	0,127	0,001	0,005	0,001
15 Red	0,300	0,293	0,098	0,100	0,072	0,070	0,008	0,003	0,003
16 Yellow	0,603	0,622	0,628	0,611	0,163	0,174	0,019	0,018	0,011
17 Magenta	0,372	0,378	0,177	0,200	0,269	0,278	0,006	0,023	0,009
18 Cyan	0,097	0,098	0,260	0,260	0,364	0,359	0,001	0,001	0,005
19 White	0,756	0,792	1,000	0,981	0,878	0,881	0,036	0,019	0,002
20 Neutral 8	0,490	0,512	0,654	0,661	0,581	0,603	0,022	0,006	0,022
21 Neutral 6.5	0,308	0,317	0,415	0,410	0,368	0,382	0,009	0,005	0,014
22 Neutral 5	0,175	0,171	0,233	0,220	0,204	0,197	0,004	0,012	0,007
23 Neutral 3.5	0,089	0,085	0,121	0,120	0,108	0,104	0,004	0,000	0,004
24 Black	0,039	0,037	0,052	0,050	0,047	0,046	0,002	0,002	0,001

2.5. CONCLUSIONS

This paper presents a methodology for determining the spectral response of photodetectors. Its efficacy was demonstrated by measuring the color directly on a standardized color palette and comparing this data with the values obtained from the simulation using the photodetector response curve found with the proposed methodology, with the reflectance curves, and with the SPD of the light source.

The applications arising from knowing the characteristic curve of low-cost photodetectors extend to all problems where it is necessary to find transformation models for output values and the simulated stimulation data is known, for example, deriving models for measurements of CCT or CRI with a color sensor using simulated spectra.

REFERENCES

[1] G. Langfelder, "Spectrally reconfigurable pixels for dual-color-mode imaging sensors," *Applied Optics*, vol. 51, no. 4, pp. A91–A98, 2012. [Online]. Available: http://dx.doi.org/10.1364/AO.51.000A91

[2] M. a. Martínez, E. M. Valero, J. Hernández-Andrés, J. Romero, and G. Langfelder, "Combining transverse field detectors and color filter arrays to improve multispectral imaging systems." *Applied optics*, vol. 53, no. 13, pp. C14–C24, 2014. [Online]. Available: http://dx.doi.org/10.1364/AO.53.000C14

[3] ASSIST, "Guide to Light and Color in Retail Merchandising," Lighthing Research Center, Tech. Rep. 1, 2010. [Online]. Available: http://www.lrc.rpi.edu/programs/solidstate/assist/

[4] K. Biron and C. Demers, "Perceptual Interactions between Light and Architecture: A graphical vocabulary using models and photographs," in *PLEA2009*, Quebec, 2009. [Online]. Available: http://www.plea2009.arc.ulaval.ca/Papers/2.STRATEGIES/2.1Daylighting/POSTER/2-1-16-PLEA2009Quebec.pdf

[5] A. Logadóttir, S. a. Fotios, J. Christoffersen, S. S. Hansen, D. D. Corell, and C. Dam-Hansen, "Investigating the use of an adjustment task to set preferred colour of ambient illumination," *Color Research & Application*, vol. 38, no. 1, pp. 46–57, Feb. 2013. [Online]. Available: http://doi.wiley.com/10.1002/col.20714

[6] F. Behar-Cohen, C. Martinsons, F. Viénot, G. Zissis, A. Barlier-Salsi, J. P. Cesarini, O. Enouf, M. Garcia, S. Picaud, and D. Attia, "Light-emitting diodes (LED) for domestic lighting: Any risks for the eye?" *Progress in Retinal and Eye Research*, vol. 30, no. 4, pp. 239–257, 2011. [Online]. Available: http://dx.doi.org/10.1016/j.preteyeres.2011.04.002

[7] H. Li, X. Mao, Y. Han, and Y. Luo, "Wavelength dependence of colorimetric properties of lighting sources based on multi- color LEDs," *Optics Express*, vol. 21, no. 3, pp. 3775–3783, 2013. [Online]. Available: http://dx.doi.org/10.1364/OE.21.003775

[8] I. Gómez, E. Pérez-Rodríguez, B. Viñegla, F. L. Figueroa, and U. Karsten, "Effects of solar radiation on photosynthesis, UV-absorbing compounds and enzyme activities of the green alga Dasycladus vermicularis from southern Spain," *Journal of Photochemistry and Photobiology B: Biology*, vol. 47, no. 1, pp. 46–57, Nov. 1998. [Online]. Available: http://www.sciencedirect.com/science/article/pii/S1011134498001997

[9] P. Pinho, T. Rosvall, E. Tetri, and L. Halonen, "Light emitting diodes in plant growth: comparative growth test in greenhouse and evaluation of photosynthetic radiation," Helsinki, 2008.

[10] W.-K. Ong, H.-F. Chen, C.-T. Tsai, Y.-J. Fu, Y.-S. Wong, D.-J. Yen, T.-H. Chang, H.-D. Huang, O. K.-S. Lee, S. Chien, and J. H.-C. Ho, "The activation of directional stem cell motility by green light-emitting diode irradiation." *Biomaterials*, vol. 34, no. 8, pp. 1911–20, Mar. 2013. [Online]. Available: http://www.sciencedirect.com/science/article/pii/S0142961212013373

[11] S. Yoshida, T. Mandel, and C. Kuhlemeier, "Stem cell activation by light guides plant organogenesis," *Genes & development*, vol. 25, no. 13, pp. 1439–50, Jul. 2011. [Online]. Available: http://www.pubmedcentral.nih.gov/articlerender.fcgi?artid=3134086&tool=pmcentrez&rendertype=abstract

[12] D. Wu and D.-W. Sun, "Colour measurements by computer vision for food quality control – A review," *Trends in Food Science & Technology*, vol. 29, no. 1, pp. 5–20, Jan. 2013. [Online]. Available: http://www.sciencedirect.com/science/article/pii/S0924224412001835

[13] S. Matta and S. Mahmud, "An intelligent light control system for power saving," in *IECON 2010-36th Annual Conference on IEEE Industrial Electronics Society*. IEEE, 2010, pp. 3316–3321. [Online]. Available: http://ieeexplore.ieee.org/xpls/abs_all.jsp?arnumber=5675331

[14] M. Miki, Y. Kasahara, T. Hiroyasu, and M. Yoshimi, "Construction of Illuminance Distribution Measurement System and Evaluation of Illuminance Convergence in Intelligent Lighting System," in *IEEE SENSORS 2010 Conference*. IEEE, 2010, pp. 2431–2434. [Online]. Available: http://mwind.doshisha.ac.jp/soe/sites/default/files/ykasahara_english.pdf

[15] Y.-J. Wen, J. Granderson, and A. Agogino, "Towards Embedded Wireless-Networked Intelligent Daylighting Systems for Commercial Buildings," *IEEE International Conference on Sensor Networks, Ubiquitous, and Trustworthy Computing*, pp. 326–331, 2006. [Online]. Available: http://ieeexplore.ieee.org/lpdocs/epic03/wrapper.htm?arnumber=1636196

[16] M. Attas, E. Cloutis, C. Collins, D. Goltz, C. Majzels, J. R. Mansfield, and H. H. Mantsch, "Near-infrared spectroscopic imaging in art conservation: investigation of drawing constituents," *Journal of Cultural Heritage*, vol. 4, no. 2, pp. 127–136, Apr. 2003. [Online]. Available: http://www.sciencedirect.com/science/article/pii/S1296207403000244

[17] E. M. Gorostiza, J. L. L. Galilea, F. J. M. Meca, D. S. Monzú, F. E. Zapata, and L. P. Puerto, "Infrared sensor system for mobile-robot positioning in intelligent spaces." *Sensors*, vol. 11, no. 5, pp. 5416–38, Jan. 2011. [Online]. Available: http://www.pubmedcentral.nih.gov/articlerender.fcgi?artid=3231390&tool=pmcentrez&rendertype=abstract

[18] Y. Le Maoult, T. Sentenac, J. Orteu, and J. Arcens, "Fire Detection," *Process Safety and Environmental Protection*, vol. 85, no. 3, pp. 193–206, Jan. 2007. [Online]. Available: http://www.sciencedirect.com/science/article/pii/S0957582007714118

[19] J. R. Mansfield, M. G. Sowa, C. Majzels, C. Collins, E. Cloutis, and H. H. Mantsch, "Near infrared spectroscopic reflectance imaging: supervised vs. unsupervised analysis using an art conservation application," *Vibrational Spectroscopy*, vol. 19, no. 1, pp. 33–45, Feb. 1999. [Online]. Available: http://www.sciencedirect.com/science/article/pii/S0924203199000041

[20] C.-C. Tong, K.-L. Wen, Y.-T. Wang, and S.-J. Lin, "The development of portable infrared color sensor," in *Industrial Technology, 2005. ICIT 2005. IEEE International Conference on*. IEEE, 2005, pp. 959–962. [Online]. Available: http://ieeexplore.ieee.org/xpls/abs_all.jsp?arnumber=1600774

[21] T. Fu, H. Zhao, J. Zeng, Z. Wang, M. Zhong, and C. Shi, "Improvements to the three-color optical CCD-based pyrometer system," *Applied Optics*, vol. 49, no. 31, pp. 5997–6005, 2010.

[22] J. E. Agudo, P. J. Pardo, H. Sánchez, A. L. Pérez, and M. I. Suero, "A low-cost real color picker based on arduino." *Sensors (Basel, Switzerland)*, vol. 14, no. 7, pp. 11 943–56, Jan. 2014. [Online]. Available: http://www.mdpi.com/1424-8220/14/7/11943

[23] G. C. Anzalone, A. G. Glover, and J. M. Pearce, "Open-source colorimeter." *Sensors (Basel, Switzerland)*, vol. 13, no. 4, pp. 5338–46, Jan. 2013. [Online]. Available: http://www.mdpi.com/1424-8220/13/4/5338/htm

[24] J. S. Bajić, D. Z. Stupar, B. M. Dakić, M. B. Živanov, and L. F. Nagy, "An absolute rotary position sensor based on cylindrical coordinate color space transformation," *Sensors and Actuators A: Physical*, vol. 213, pp. 27–34, Jul. 2014. [Online]. Available: http://www.sciencedirect.com/science/article/pii/S0924424714001617

[25] K.-C. Lee, S.-H. Moon, B. Berkeley, and S.-S. Kim, "Optical feedback system with integrated color sensor on LCD," *Sensors and Actuators A: Physical*, vol. 130-131, pp. 214–219, Aug. 2006. [Online]. Available: http://www.sciencedirect.com/science/article/pii/S0924424706000495

[26] M. Moghavvemi, S. S. Jamuar, E. H. Gan, and Y. C. Yap, "Design of low cost flexible RGB color sensor," in *2012 International Conference on Informatics, Electronics & Vision (ICIEV)*, IEEE, Ed. Dhaka: IEEE, May 2012, pp. 1158–1162. [Online]. Available: http://ieeexplore.ieee.org/xpls/abs_all.jsp?arnumber=6317416http://ieeexplore.ieee.org/lpdocs/epic03/wrapper.htm?arnumber=6317416

[27] O. G. Saracoglu and H. Altural, "Color Regeneration from Reflective Color Sensor Using an Artificial Intelligent Technique," *Sensors (Basel, Switzerland)*, vol. 10, no. 9, pp. 8363–8374, Sep. 2010. [Online]. Available: http://www.mdpi.com/1424-8220/10/9/8363/

[28] A. Sen, J. Albarella, J. Carey, P. Kim, and W. McNamara III, "Low-cost colorimetric sensor for the quantitative detection of gaseous hydrogen sulfide," *Sensors and Actuators B: Chemical*, vol. 134, no. 1, pp. 234–237, Aug. 2008. [Online]. Available: http://linkinghub.elsevier.com/retrieve/pii/S0925400508003171

[29] M. Aldrich, N. Zhao, and J. A. Paradiso, "Energy efficient control of polychromatic solid state lighting using a sensor network," in *SPIE 7784, Tenth International Conference on Solid State Lighting*. SPIE, Aug. 2010. [Online]. Available: http://proceedings.spiedigitallibrary.org/proceeding.aspx?articleid=754196

[30] M. Ashibe, M. Miki, and T. Hiroyasu, "Distributed optimization algorithm for lighting color control using chroma sensors," in *2008 IEEE International Conference on Systems, Man and Cybernetics*. Singapore: IEEE, Oct. 2008, pp. 174–178. [Online]. Available: http://ieeexplore.ieee.org/lpdocs/epic03/wrapper.htm?arnumber=4811270

[31] J.-S. Botero V., F.-E. López G., and J.-F. Vargas B., "Calibration method for Correlated Color Temperature (CCT) measurement using RGB color sensors," in *Image, Signal Processing, and Artificial Vision (STSIVA), 2013 XVIII Symposium of*. Bogotá: IEEE, 2013, pp. 3–8. [Online]. Available: http://ieeexplore.ieee.org/xpls/abs_all.jsp?arnumber=6644921

[32] ——, "Calibration Method for Measuring the Color Rendering Index (CRI) using RGB Sensor," *Tecnológicas*, vol. EE, pp. 325–338, 2013.

[33] J.-S. Botero V., S.-M. Navarro, N. Giraldo, and L. Atehortua, "Estimation of Photosynthetically Active Radiation (PAR) using a low cost spectrometer," *IEEE Latin America Transactions*, vol. 12, no. 2, pp. 107–111, Mar. 2014. [Online]. Available: http://ieeexplore.ieee.org/lpdocs/epic03/wrapper.htm?arnumber=6749525

3

CAMERA CALIBRATION

Contents

3.1. ABSTRACT

Digital cameras are photodetector arrays that respond to particular bands of the electromagnetic spectrum, and specifically those in the visible spectrum between 380 and 780 nm are the most commonly used. The main cameras function is store the image from an aesthetic point of view, when these are used in home applications. For this reason, several processes are used in image reconstruction to improve the visual appearance, even from manufacturing process of sensor decreasing the possibility to obtain optical measurements with this cameras. However, digital cameras can also be used as optical measuring instruments knowing their features in depth. Therefore, in this paper is proposed a calibration method for monochrome digital camera using a monochromator and an automatic rotation system. In this way, the uniformity of the pixels response is verified, bad pixels are detected, and the sensitivity curve is obtained. The results show the advantages of the method to find regions of pixels turned off. Also, the value of sensitivity in function of wavelength is obtained to verify the regions with significant changes of uniformity. This work aims to the prototyping of a color measurement system and it is very important a comprehensive understanding of the camera.

3.2. INTRODUCTION

Digital cameras are developed using photosensors array. This array is built with individual sensors which can be Charge-Coupled Device (CCD) or Complementary Metal-Oxide-Semiconductor (CMOS). The array size has been increased and the total sensor area significantly has been reduced in recent years in order to improve the resolution. Also, with the objective of achieving a better image reproduction the color filter mosaic (CFM) and processing techniques are developed. In general, the largest application segment for cameras is the reproduction of scenes from an aesthetic point of view, causing that their development is oriented to improve the appearance, but not the quality of the measures in the image. Technological development has allowed the access to image acquisition devices of good quality and reasonable cost, encouraging the development of systems based on image processing and analysis. It is no secret that image analysis has become an important tool in a wide range of areas, ranging from everyday situations to specific applications in the industry, medicine, biology, chemistry, among others. In this sense, digital cameras have facilitated the image recording and improved the quality of them.

In particular, the use of digital cameras for color measurement has proved to be useful in several applications. For example, some researches areas are food quality analysis [1–5], UVI indication [6], determination of glucose in urine [7], determination of plant nutrients in soil [8], fish spoilage monitoring [9], and other applications in analytical chemistry [10, 11]. However, color distortion is a common problem, even the same camera captures different colors of the same scene in different times. Although the scene also depends capture conditions of the image. Indeed, in a monochromatic scene the pixels within an image could vary the intensity measured. This happens because each camera light sensors (photosensors or photodetectors) produces differents response to the same stimulus, or because of defective regions in the array.

A strategy used for color calibration is to create a database with color images and their respective labels. New images are acquired and compared with the stored images in the database in order to determine its category [10]. Other proposals employ Color Checkers, color arrays, and color-encode fringe patterns, to establish the relation between the measured color and the real color, and generate a way to correct the measured color if necessary [8, 12–14]. Usually, the goal is to obtain a reliable measure, nevertheless, these approaches require a lot of experimental work and the results may be biased because it is not feasible to consider all capture conditions (e.g. all possible light sources).

The objective of this work is to find the characteristic curve of a digital camera, find defective pixels, and evaluate the uniformity of the response starting from a broadband light source. The authors have developed similar works [15], but only to estimate the sensitivity curve in individual photodetectors. The generated light is introduced in a monochromator to ensure a specific wavelength. After this, the light is divided to feed a power meter and the photodetector surface simultaneously. The wavelength of the monochromator is varied in the range of visible light (380 nm to 780 nm) using 20 nm increments to generate curves of 21 points for each photodetector.

3.3. MATERIALS AND METHODS

3.3.1. CAMERA FL3U313Y3MC

FL3-U3-13Y3M-C (Figure 3.1) is a monochromatic camera developed by FLIR with excellent performance. One of the main advantages of this type of cameras compared to those with domestic use is the availability of data in raw format. This allows to directly obtain the response of the sensors without processing, and this is a necessary characteristic to use the camera as a measuring element and all control parameters are known and operated manually.

Figure 3.1 Camera FL3U313Y3MC

3.3.2. EXPERIMENT DESCRIPTION

In Figure 3.2 the explanatory diagram of the proposed experiment is presented and its parts are described below:

1. The initial response value to obtain the saturation parameters is adjusted with light emitted at 525 nm.
2. The system input is a white light source EQ-99 (polychromatic) with UV-VIS-NIR emission (1) coupled to the monochromator (2) via optical fiber.
3. The white light inside to the mechanical UV-VIS-NIR monochromator (2) (Mini-Chrom) that selects the desired wavelength. The adjustment of the wavelength is carried out manually with a mechanical element in increments of 20 nm in the visible spectrum (380-780 nm). The light output of the monochromator is a 300 um slit.
4. The output of the monochromator illuminates an area. The camera (3) is positioned in such a way that the surface of the sensor is completely covered by monochrome light. The power of the light is also measured (4) using the spectrometer at the same plane where the sensor is located.
5. The camera (3) is mechanically coupled to a digital servomotor that moves it automatically on 6 different angles for each wavelength. The camera is rotated to detect problems of uniformity of the light source, that is, a defective pixel pattern should be seen even if the camera is rotated and this shows that it is not due to a projected light problem. In order to determine the efficiency of the sensor, the power is taken in the measurement plane at 525 nm and the camera is moved near or far as appropriate to match the power at 525 nm for each wavelength. This task must be performed due to the uncertainty in the elements used to process the light.
6. The values obtained in the previous steps will allow to know the photodetector efficiency on certain wavelength, the uniformity in the pixels response, and detect the defective pixels in the array.

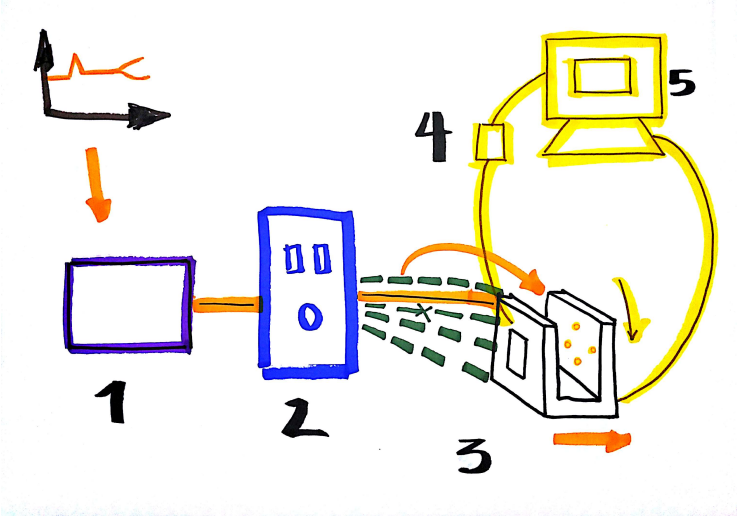

Figure 3.2 Experiment description

3.3.3. CALIBRATION METHOD

The compressed image storage formats make undetectable the defects on the sensors, because the processing operations repair or camouflage the pixels with information from the region. For this reason, the images used in this experiment are acquired in raw format due to the camera is used as a measurement element.

The method proposed in this work provides information on the operation of the sensor. The quality of the parameters must be adjusted for each experiment where the camera is used as a measurement element. For example, the number of defective pixels tolerated is a dependent value in the application, that is, the percentage of pixels that are allowed to be defective. The images obtained using the experiment described in the previous subsection can be calibrated with the three steps process described below:

1. First, the mean and standard deviation are calculated for each of 105 images acquired in the experiment. The average value of the images reflects the power absorbed by the photodetectors array, however, the values in defective pixels are deviated of the average. In this step, pixels with two deviations above or below of the mean are selected as defective pixels, this value reached 0.1% of the photodetector pixels in the worst case. Defective pixels must be aligned between images with different angles to decrease the error in the experiment. These pixels do not provide information to the image, their response does not change to different stimulus, or it is substantially different to the rest of pixels. Defective pixels are detected and marked to not use them.

2. It is desirable to know the uniformity of the pixel response, that is, how similar is the response of the pixels if they are stimulated with the same power. Several imperfections in the camera con not be eliminate in the experiment results, and consequently these can affects the uniformity of the power that is arriving on the sensor. The rotation is again used as a tool to calculate the uniformity. It is possible to know a approximated response of a pixel by calculating the average of five rotated images for each wavelength. For this way, each pixel is exposed to five different points of the projection plane of the monochromator. The result is a averaged image which is used to calculate the range of sensor response for each wavelength. The source which the pixels are exposed comes from monochromator and it is assumed uniform.

3. The sensitivity curve of the camera is obtained. For this, the axial displacement of the system was used to ensure that the detector surface would always be exposed to the same power at 525 nm. In view of this, the mean value of each of the 105 images was used to delete the defective pixels. The values are represented in a Cartesian system where the x-axis is the wavelength and the y-axis is the mean value of each image. With these points, a curve that represents the experimental dispersion is calculated, and the sensitivity curve of the camera is obtained. A interpolated curve allows to estimate the sensor response at any wavelength.

3.4. RESULTS AND DISCUSSIONS

3.4.1. DETECTION OF DEFECTIVE PIXELS

In order to determine defects on the sensor surface, the mean and standard deviation of the response values for each image are calculated. Then, the pixels with two deviations above or below of the mean are selected. The results are shown in Figure 3.3, where P1, P2 and P3 are rotation positions, the images are shown for two wavelengths 460 nm and 740 nm. The white regions in figure highlight the defective pixels, 227 defective pixels were detected. The purpose of camera rotation is that defective pixels appear in the same region facilitating their localization, and other regions produced by other different phenomenons are discarded. The set of highlighted pixels must be excluded when the sensor is used as a measurement element. It is important to note that the images have artificial color to facilitate their interpretation.

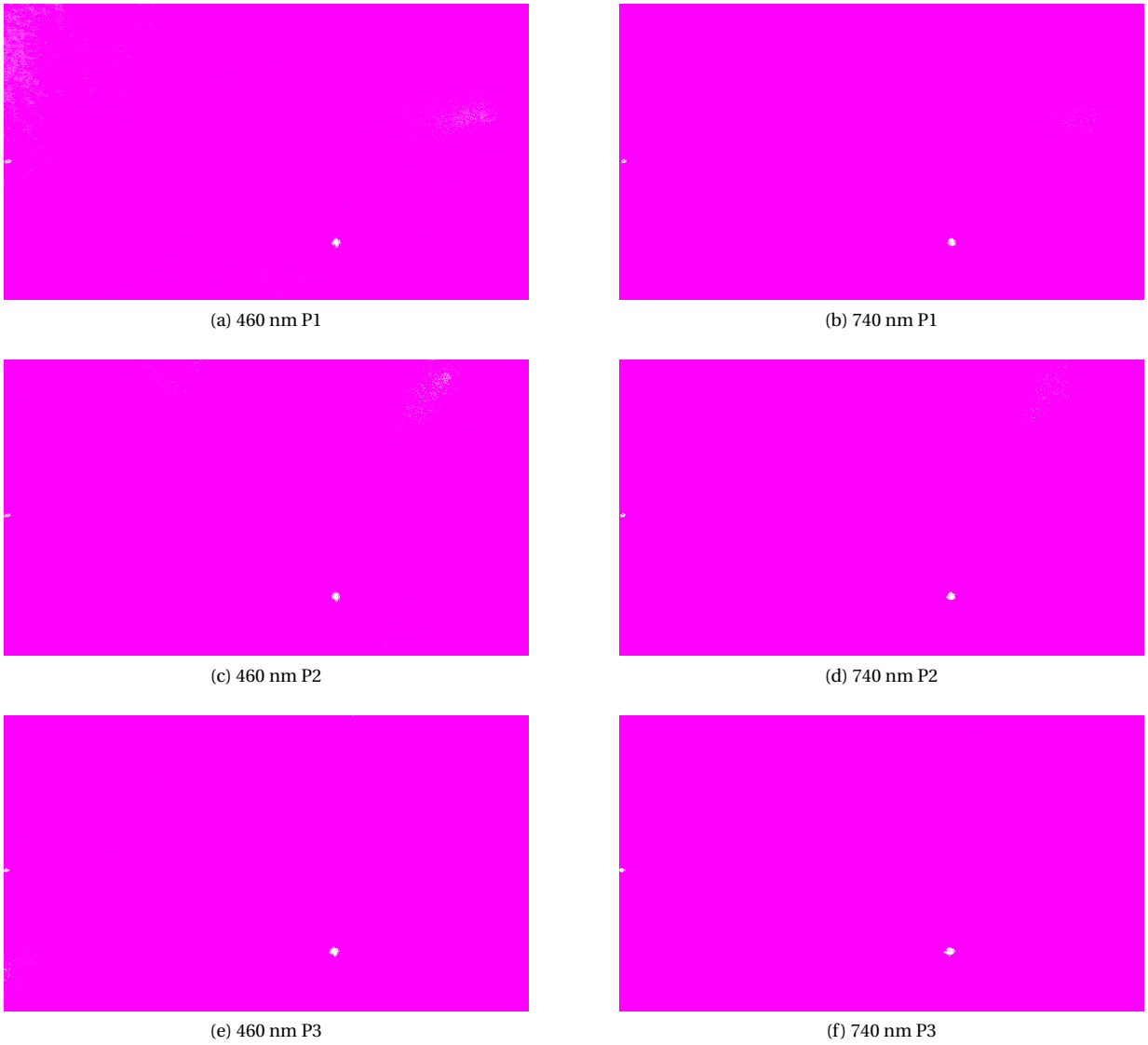

(a) 460 nm P1

(b) 740 nm P1

(c) 460 nm P2

(d) 740 nm P2

(e) 460 nm P3

(f) 740 nm P3

Figure 3.3 Detection of defective pixels

3.4.2. ESTIMATION OF UNIFORMITY

Figure 3.4 shows the raw response of the photodetector for different rotation positions (P1 and P5) and different wavelengths (480 and 640). In total the 5 images of each wavelength are averaged to calculate the resulting image Pm. It can be seen that uniformity improves. On this image, the response range for each wavelength is estimated. The intensity in the figures is normalized between the pixel with the lowest value and the pixel with the highest value, for this reason, each experiment has its own scale.

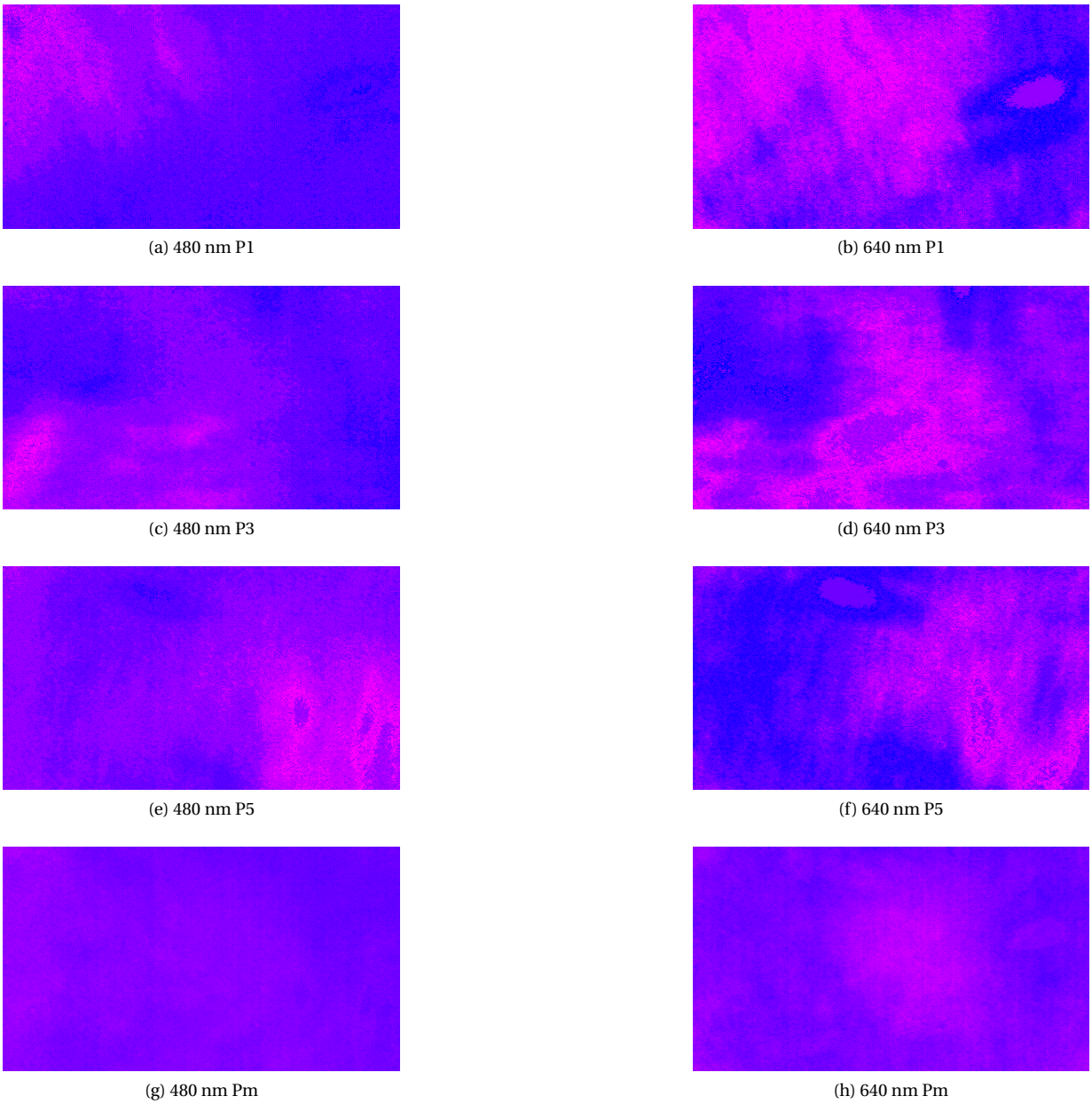

(a) 480 nm P1

(b) 640 nm P1

(c) 480 nm P3

(d) 640 nm P3

(e) 480 nm P5

(f) 640 nm P5

(g) 480 nm Pm

(h) 640 nm Pm

Figure 3.4 Estimation of uniformity

3.4.3. SENSITIVITY ESTIMATION

Measurements of spectra were taken every 20 nm in the range between 380 nm and 780 nm having 21 spectra in total. The uncertainty due to the orthogonality of the sensor plane when is illuminated, and non-uniformity of light of the monochromator output are reduced repeating the measurement five times in diferent angles. As shown in Figure 3.5, the spectra are narrow allowing improve the estimation of the response model generated. Also, as mentioned in the the description of the experiment, the camera is moved near or far of the monochromator as appropriate to match with the power at 525 nm for each wavelength with the help of the spectrometer, as explained in the section 3.3.2.

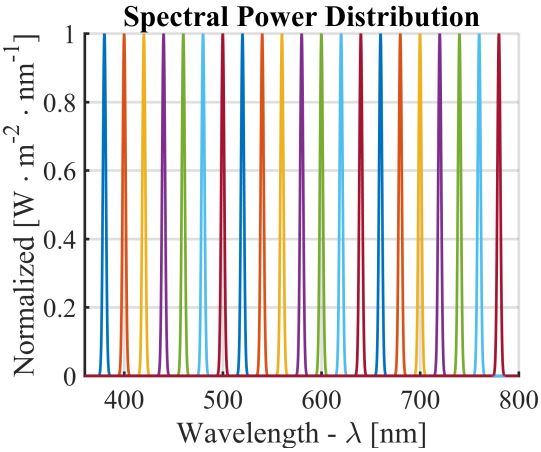

Figure 3.5 Output monochromator

The mean of each image in each rotation position is obtained in this step and the mean for each evaluated wavelength of each rotated images is represented by the red dots, see Figure 3.6. The power that reaches the camera in each wavelength was equal, for this reason the values are normalized with respect to the maximum of the digital response of the camera.

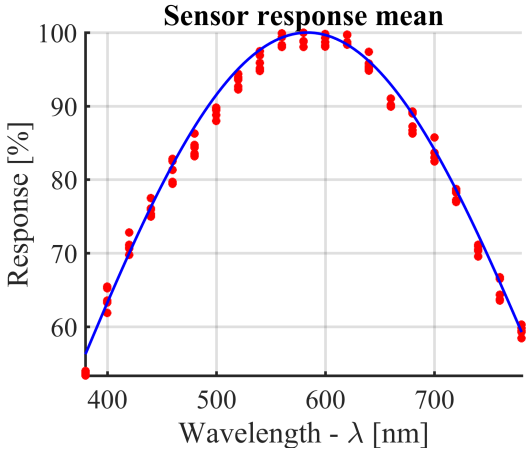

Figure 3.6 Sensor sensitivity

Equation 3.1 presents the estimated sensitivity function of the camera (blue line in 3.6), where the parameter k must be adjusted with the power. The adjustment allows interpolating the response in sensitivity of the sensor to unmeasured values.

$$S(\lambda) = k \cdot (1.2\text{E}-08 \cdot \lambda^4 - 2.8E-05 \cdot \lambda^3 + 0.02 \cdot \lambda^2 - 5.7 \cdot \lambda + 544.4) \tag{3.1}$$

Finally, in Table 3.1, the average value of each image for each position (P1, P2, P3, P4, P5) and each of the 21 sampled wavelengths is presented, that is, the averages of the figure 3.6 for each wavelength. The value is normalized from 0 to 100 %, the last column shows the response range of the camera (Margin), which represents the maximum difference for the specific wavelength.

Table 3.1 Mean response and margin

Wavelength [nm]	P1 [%]	P2 [%]	P3 [%]	P4 [%]	P5 [%]	Margin [%]
380	53.34	53.95	53.56	53.78	53.70	0.62
400	63.33	61.86	65.23	65.44	63.52	3.58
420	71.15	70.64	72.82	70.74	69.75	3.07
440	77.50	75.92	75.33	76.05	74.95	2.55
460	79.70	82.51	82.83	81.34	79.45	3.39
480	84.35	84.73	86.25	83.23	83.53	3.02
500	87.98	89.80	89.78	89.45	88.78	1.82
520	93.61	92.64	94.40	92.27	93.87	2.13
540	95.13	95.90	96.91	97.45	94.78	2.67
560	99.87	99.35	98.29	98.04	98.07	1.83
580	98.02	98.79	98.84	100.00	100.00	1.98
600	99.26	98.23	99.80	98.71	98.07	1.72
620	99.73	99.67	98.34	98.68	98.50	1.39
640	94.84	95.38	95.80	95.05	97.37	2.53
660	89.98	90.09	89.93	90.13	91.01	1.09
680	86.70	89.26	87.22	86.27	89.00	2.98
700	85.73	83.66	82.46	83.01	83.67	3.27
720	78.47	77.22	78.23	78.72	76.97	1.74
740	69.53	70.47	70.32	70.95	71.12	1.60
760	63.61	64.32	66.50	63.67	66.72	3.11
780	60.26	59.40	59.78	58.43	59.26	1.83

3.5. CONCLUSIONS

The proposed method shows the detection of defective pixels (find regions of pixels off) using the experimental design, estimates the sensitivity values as a function of the wavelength, and verify the uniformity of the pixels response in a photodetector array. The two results are used in combination to use the photodetector as a measurement tool. The sensitivity is used to derive power measurements, and the defective pixels to know regions that should not be used in the measurement.

The results show that it is necessary to develop the process described in this work because it is common for sensor arrays to be found, defective pixels and as it is known their sensitivity is far from uniform, the sensitivity curve is fundamental if wants to use the camera as a measuring element, taking into account that the spectral characteristics of the cameras are different and that when obtaining the response in sensitivity, the sensor can be used as a measurement element at any wavelength, compensating with the adjusted curve.

As mentioned, the aim of this work is to acquire information that allows the camera to be used as a measurement element. With the information obtained, it is expected that the camera can be used in color measurement systems, particularly when hyperspectral sources are used and the camera is used to measure reflectance.

REFERENCES

[1] D. Wu and D.-W. Sun, "Colour measurements by computer vision for food quality control – A review," *Trends in Food Science & Technology*, vol. 29, no. 1, pp. 5–20, 2013.

[2] D.-J. Lee, J. K. Archibald, and G. Xiong, "Rapid Color Grading for Fruit Quality Evaluation Using Direct Color Mapping," *IEEE Transactions on Automation Science and Engineering*, vol. 8, no. 2, pp. 292–302, apr 2011.

[3] J. V. Popov-Raljić and J. G. Laličić-Petronijević, "Sensory Properties and Color Measurements of Dietary Chocolates with Different Compositions During Storage for Up to 360 Days," *Sensors*, vol. 9, no. 3, pp. 1996–2016, 2009.

[4] M. Amensour, E. Sánchez-zapata, J. Abrini, and E. Sendra, "Estabilidad del color en salchichas de pollo tipo Frankfurt adicionadas con extracto acuoso de hoja de Myrtus communis," *Óptica pura y aplicada*, vol. 43, no. 4, pp. 251–257, 2010.

[5] Z. Xiao-bo, Z. Jie-wen, L. Yanxiao, and M. Holmes, "In-line detection of apple defects using three color cameras system," *Computers and Electronics in Agriculture*, vol. 70, no. 1, pp. 129–134, 2010.

[6] Q. Meng, L. Fang, T. Han, S. Huang, and S. Xie, "A photochromic UVI indication card and the colorimetric analysis system built on smartphones," *Sensors and Actuators B: Chemical*, vol. 228, pp. 144–150, jun 2016.

[7] M. Y. Jia, Q. S. Wu, H. Li, Y. Zhang, Y. F. Guan, and L. Feng, "The calibration of cellphone camera-based colorimetric sensor array and its application in the determination of glucose in urine," *Biosensors and Bioelectronics*, vol. 74, pp. 1029–1037, 2015.

[8] N. Moonrungsee, S. Pencharee, and J. Jakmunee, "Colorimetric analyzer based on mobile phone camera for determination of available phosphorus in soil," *Talanta*, vol. 136, pp. 204–209, 2015.

[9] M. K. Morsy, K. Zór, N. Kostesha, T. S. Alstrøm, A. Heiskanen, H. El-Tanahi, A. Sharoba, D. Papkovsky, J. Larsen, H. Khalaf, M. H. Jakobsen, and J. Emnéus, "Development and validation of a colorimetric sensor array for fish spoilage monitoring," *Food Control*, vol. 60, pp. 346–352, feb 2016.

[10] P. Masawat, A. Harfield, and A. Namwong, "An iPhone-based digital image colorimeter for detecting tetracycline in milk," *Food Chemistry*, vol. 184, pp. 23–29, 2015.

[11] L. F. Capitán-Vallvey, N. López-Ruiz, A. Martínez-Olmos, M. M. Erenas, and A. J. Palma, "Recent developments in computer vision-based analytical chemistry: A tutorial review," *Analytica Chimica Acta*, vol. 899, pp. 23–56, oct 2015.

[12] R. Gong, Q. Wang, X. Shao, and J. Liu, "A color calibration method between different digital cameras," *Optik - International Journal for Light and Electron Optics*, vol. 127, no. 6, pp. 3281–3285, 2016.

[13] W. Li and S. Duan, "Color calibration and correction applying linear interpolation technique for color fringe projection system," *Optik - International Journal for Light and Electron Optics*, vol. 127, no. 4, pp. 2074–2082, 2016.

[14] R. Shrestha, A. Mansouri, and J. Y. Hardeberg, "Multispectral imaging using a stereo camera: concept, design and assessment," *EURASIP Journal on Advances in Signal Processing*, vol. 2011, no. 1, p. 57, dec 2011.

[15] J.-S. Botero V., F.-E. Lopez G., and J.-F. Vargas B., "Characterization of photodectors using a monochromator and a broadband light source in the XYZ color space," *International Journal on Smart Sensing and Intelligent Systems*, vol. 9, no. 2, pp. 752–764, 2016. [Online]. Available: http://s2is.org/Issues/v9/n2/papers/paper18.pdf

4

ESTIMATION OF LIGHT INDEX

Contents

4.1. ABSTRACT

Artificial light sources have been essential in the social and economic development of humanity. At first, light sources were evaluated only in function of the emitted power but nowadays additional indicators are considered such as the Color Rendering Index, the Gamut Area, among others. These features have been related to the development of new models that allow to control polychromatic sources for modifying the color reproducibility characteristics, and this leads to the necessity of low cost sensing models that allow to estimate this parameters to interact with control systems in real time. Furthermore, the problem is that in most natural settings multiple light sources can be overlapped, increasing the model complexity. For this reason, in this work it is presented a method to estimate the CRI and GA, which it's adapted with the characteristic curves of a RGB sensor of general purpose using Deep Learning. To this end, the model is trained with a dataset created with combinations of 125496 spectra. The variables of the RGB sensor and 6 linear and nonlinear combinations of them, are considered as inputs. Results show that the indices can be estimated with an absolute error lower than 2% in both cases.

4.2. INTRODUCTION

Artificial light has been, since its invention, fundamental for the economic development of society and of great importance in the quality of life, it is almost impossible to imagine the world without the presence of electric light sources. Initially, fuel sources were developed (which are highly contaminant), but they quickly evolved to electric sources that are significantly easier to handle and increasingly efficient considering the absorbed energy that is finally converted into light.

The power consumption is highly related to the light sources, according to the "2010 U.S. Lighting Market Characterization"[1], there were 8.2 billion lamps installed in the United States with an approximate consumption of 700 TWh, of which 175 are for the residential sector, 349 for the commercial sector, 58 for the industry and 118 for outdoor lighting. In that sense, it has been necessary the evolution of light sources regarding energy efficiency [2], the development of complex models for lighting control [3, 4], the evaluation of external conditions that originally were not taken into account (like the color of the walls [5], the color of the windows [6], the color rendering transmission in objects seen by an observer outside a building [7], among others), and the development of studies and methods to characterize in more detail the light sources [8]. Also, there have been important models of energy consumption in the residential sector [9], that served to assess the impact of LED sources in households with significant results.

There is a tendency to replace incandescent, halogen and fluorescent sources with LED light sources [10–12], mainly because this represent a considerable reduction in electricity consumption. Although it is important to know that there are works that warn about the potential risk to the human eye when using LEDs as sources of white light [13] and it should be known that further studies are required to clearly define its limits. The construction of RGB LEDs allows them to be individually adjustable, making possible to control the chromaticity and enabling application development like in [14] were through LED arrays, uniform illumination patterns can be created and [15] where are presented the advantages in the implementation of a control model and RGB sensors are used (as in this paper). In the same line, theoretical models of narrowband emitters have been developed to build sources with high CRI [16] and LED sources with high Gammut Area (GA) [17] for retail lighting. Also, important works have been developed to implement controllers at the power electronics level with temperature compensation [18]. Close to the LED field, currently there is a research line where models are sought to allow a better perception of different types of scenes, as in [19] where intercultural lighting preferences were evaluated (Germany, China), which is similar to the work presented in [20], but in this case the America–China intercultural comparison is made and evaluated on art pieces.

In general, there are numerous studies found in the literature that highlight the relevance of visual assessment of light sources [21–24], being the commercial sector the one with highest energy consumption and where color reproduction capability is more important. Several works have been developed for presenting recommendations on sources selection [25, 26], and specific works where sources are evaluated for better perception in commercial environments [17, 27].

On the other hand, the Deep Learning (DL) comprises of a group of machine learning techniques that allows modeling data with high level of abstraction using composite architectures, which as in the case presented in this paper allows mapping complex nonlinear spaces to derive indirect measures in inexpensive sensors. The DL has been extensively studied and analyzed, at present, high-quality literature can be found to understand its use and multiple fields of application, which proves DL usefulness for solving modeling and prediction problems. This kind of techniques have been used deeply in troubleshooting computer vision [28, 29], also for modeling time series [30], in electrocardiographic signals classification [31], in manufacturing [32], water distribution systems [33], consumption models [34], prediction of energy consumption in buildings [35], in mapping wind profiles with information to other areas [36], among many other applications. RGB sensor characterization has been studied from different points of view, using controlled conditions and reference measurements to calibrate from the wavelength (being this a more generalizable model) [37, 38] , or mapping methods from examples that might over fit the problem [39–43].

The CRI index is a measure used to represent perceptual color reproducibility of a source, it could be seen as the proximity to the white of a particular light source. The use of this index is still under discussion and works have been done to compare with more complex indices. Another index used to characterize light sources nowadays is the Gamut Area Index, the higher the GAI, the greater the saturation of the colors. The CRI and the GAI are calculated from the SPD (Spectral Power Distribution) of the light source, so that a spectrometer (relatively

expensive equipment) is needed, besides that it is possible to have dynamic measurements and to carry out control applications from the indices, as intended with the implementation proposed in this article. For this reason, in this paper, a methodology for estimating the CRI and GAI using the information provided by low-cost RGB sensors with a Multi-Layer Perceptron (MLP) is presented. To validate the effectiveness of the methodology, the estimation error was evaluated for two different commercial sensors (TCS3414CS and ADJDS311) and as well the compromise between error and training time. In total, 640 Multi-Layer Perceptron architectures were trained by varying the number of layers, the number of neurons per layer, the activation function and the calculation architecture (CPU vs GPU) that significantly affects the training time and is reflected in the estimation error due to the use of the floating point. In addition, as a contribution to this work, a database was built with more than 120,000 combined source spectra (artificial and sun light) that will serve as a reference for developing new estimation methods.

Finally, the results show the effectiveness of the method to train an MLP with an absolute error lower than 2 to estimate the GAI and the CRI with both sensors. The purpose of this result is to use low cost sensors as estimators in measurement nodes in automatic lighting control in environments where the reproducibility characteristics of lighting are required to be stable by combining available sources with polychromatic sources. Also in the estimation of disturbances in environments where color is measured using controlled light sources.

4.3. MATERIALS AND METHODS

4.3.1. COLOR SENSOR TCS3414CS

TCS3414CS is a color sensor manufactured by Texas Advanced Optoelectronic Solutions (TAOS). It comprises of an 8x2 array of filtered photodiodes, four of them have red filters, four blue, and four green ones; the remaining four are not filtered. Each of the four sensor channels (Red, Green, Blue, Clear) delivers its output in a format of 16 bits using I2C protocol information at 400 KHz. The gain of the analog converter and the integration time are programmable. Table 4.1 shows some important features of TCS3414CS.

Table 4.1 Characteristic TCS3414CS

Characteristic	*Value*	*Units*
Sensor	*Photodiode*	[NA]
Clock frequency	0-400	[KHz]
A/D Resolution	16	[bits]
Channels	*R, G, B, clear*	[NA]

4.3.2. COLOR SENSOR ADJDS311

The ADJDS311 is a color sensor manufactured by Avago Technologies. This one is made of a 7x6 array of filtered photodiodes, ten of which have red filters, ten blue ones, and ten green ones, the remaining ten are not filtered. Each one of the four sensor channels (Red, Green, Blue, and Clear) delivers its output in a format of 10 bits using I2C protocol information at 100 KHz. The sensitivity is controlled via a serial interface and can be optimized for the different color channel. Table 4.2 shows some important features of the ADJDS311 photo sensor. The sensor can be used in conjunction with a white LED for measuring the color on surfaces. It does not need an external capacitor.

Table 4.2 Characteristic ADJDS311

Characteristic	*Value*	*Units*
Sensor	*Photodiode*	[NA]
Clock frequency	0-100	[KHz]
A/D Resolution	10	[bits]
Chanels	*R, G, B, clear*	[NA]

4.3.3. CCT, CRI AND GA CALCULATION

In this section the manual form of calculation of the indices estimated in this work is presented. It is clear that in order to construct the reference value for each of the 125496 analyzed sources it was necessary to apply this calculation to each one in order to construct the training set.

The CIE X, Y and Z coordinates of a light source can be calculated using the Spectral Power Distribution (SPD) of the light source and the CIE Standard Observer matching functions. As mentioned above, the main problem of applying the direct calculation method is need the SPD and a spectrometer. The equations are presented in (4.1), where K is a constant for normalized Y to 100.

$$\begin{aligned} X &= K \sum_{\lambda=380}^{780} SPD(\lambda) \cdot \tilde{x}(\lambda) \\ Y &= K \sum_{\lambda=380}^{780} SPD(\lambda) \cdot \tilde{y}(\lambda) \\ Z &= K \sum_{\lambda=380}^{780} SPD(\lambda) \cdot \tilde{z}(\lambda) \end{aligned} \tag{4.1}$$

The chromaticity coordinates x, y can be obtained from X, Y and Z values. These equations are presented in (4.2).

$$\begin{aligned} x &= \frac{X}{X+Y+Z} \\ y &= \frac{Y}{X+Y+Z} \end{aligned} \tag{4.2}$$

Later, with the equations shown in [44], the Correlated Color Temperature (CCT) is estimated. The equations are presented in (4.3).

$$\begin{aligned} n &= \frac{x-0.3320}{0.1858-y} \\ CCT &= 449n^3 + 3525n^2 + 6823n + 5520 \end{aligned} \tag{4.3}$$

The next step is to determine the reference illumination based on the CCT of the light source. The reference light has the same CCT as the light source of interest, which is calculated using equation (4.4) if the value of $CCT < 5000K$ or using the model presented in (4.5), in otherwise. In (4.5), h is the Planck constant, c is the light speed, k is the Boltzmann constant and λ is the wavelength.

$$SPD_{Ref} = \frac{2\pi hc^2 \left(10^{-9}\lambda\right)^{-5}}{e^{\left(\frac{hc}{CCT \cdot 10^{-9}\lambda k}\right)} - 1} \tag{4.4}$$

For $CCT \geq 5000K$, the reference light can be calculated as shown in (4.5), where $S_0(\lambda)$, $S_1(\lambda)$ and $S_2(\lambda)$ are vectors of the distribution of daylight.

$$
\begin{aligned}
&SPD_{Ref}(\lambda) = S_0(\lambda) + [M_1 \cdot S_1(\lambda)] + [M_2 \cdot S_2(\lambda)] \\
&M_1 = \frac{-1.3515 - 1.7703 \cdot x_D + 5.9114 \cdot y_D}{0.0241 + 0.2562 \cdot x_D - 0.7341 \cdot y_D} \\
&M_2 = \frac{0.0300 - 31.4424 \cdot x_D + 30.0717 \cdot y_D}{0.0241 + 0.2562 \cdot x_D - 0.7341 \cdot y_D} \\
&CCT \leq 7000K \\
&x_D = -\frac{4.6070 \cdot 10^9}{T_C^3} + \frac{2.9678 \cdot 10^6}{T_C^2} + \frac{0.09911 \cdot 10^3}{T_C} + 0.244063 \\
&7000K < CCT \leq 25000K \\
&x_D = -\frac{2.0064 \cdot 10^9}{T_C^3} + \frac{1.9018 \cdot 10^6}{T_C^2} + \frac{0.24748 \cdot 10^3}{T_C} + 0.237040 \\
&y_D = -3.000 \cdot x_D^2 + 2.870 \cdot x_D - 0.275
\end{aligned}
\tag{4.5}
$$

Then the values of CIE 1976 (u', v') are determined for each of the eight color samples (TCS), for this it is necessary to calculate the XYZ values first, both as a source of interest and as the reference illumination values for each (X, Y and Z),as shown in (4.6).

$$
\begin{aligned}
X_i &= K \sum_{\lambda=380}^{780} SPD(\lambda) \cdot \tilde{x}(\lambda) \cdot TCS_i(\lambda) \\
Y_i &= K \sum_{\lambda=380}^{780} SPD(\lambda) \cdot \tilde{y}(\lambda) \cdot TCS_i(\lambda) \\
Z_i &= K \sum_{\lambda=380}^{780} SPD(\lambda) \cdot \tilde{z}(\lambda) \cdot TCS_i(\lambda)
\end{aligned}
\tag{4.6}
$$

Now the CIE 1976 (u', v') values are derived for each TCS using (4.7). As will be seen later, these values are used in GA calculation. It is important to understand that each combination u', v', represents the correlation with a particular TCS and could be viewed as the abstraction of the proximity to a particular color source.

$$
\begin{aligned}
u' &= \frac{4X}{X + 15Y + 3Z} \\
v' &= \frac{6X}{X + 15Y + 3Z}
\end{aligned}
\tag{4.7}
$$

The adaptive color shift *Von Kries* is applied to respect the differences between the states of the chromatic adaptation of the light source of interest and the reference illumination as shown in (4.8). The c and d values are calculated for all the reference sources.

$$
\begin{aligned}
c &= \tfrac{1}{v}\left(4-u'-10v'\right)\\
d &= \tfrac{1}{v}\left(1.708v'+0.404-1.481u'\right)\\
u_{k,i} &= \frac{10.872+0.404\frac{c_{ref}}{c_k}c_{k,i}-4\frac{d_{ref}}{d_{k,i}}d_{k,i}}{16.518+1.481\frac{c_{ref}}{c_k}c_{k,i}-\frac{d_{ref}}{d_{k,i}}d_{k,i}}\\
v_{k,i} &= \frac{5.520}{16.518+1.481\frac{c_{ref}}{c_k}c_{k,i}-\frac{d_{ref}}{d_{k,i}}d_{k,i}}
\end{aligned}
\tag{4.8}
$$

Now, the CIE 1964 $U*W*V$ values are determined for each TCS (4.9).

$$
\begin{aligned}
W_i^* &= 25\cdot {Y_i}^{1/3}-17\\
U_i^* &= 13\cdot W_i^*\cdot(u_i-u)\\
V_i^* &= 13\cdot W_i^*\cdot(v_i-v)
\end{aligned}
\tag{4.9}
$$

Finally the color shift is determined ΔE for each TCS, using the equation (4.10).

$$
\Delta E_i=\sqrt{(U^*_{ref,i}-U^*_{k,i})^2+(V^*_{ref,i}-V^*_{k,i})^2+(W^*_{ref,i}-W^*_{k,i})^2}
\tag{4.10}
$$

And with these values of ΔE_i the R_i and average CRI (4.11) are calculated.

$$
\begin{aligned}
R_i &= 100-4.6\Delta E\\
CRI &= \tfrac{1}{8}\sum_{i=1}^{8}R_i
\end{aligned}
\tag{4.11}
$$

Now to calculate the Gamut Area (GA) we return to equation (4.7), with this the CIE 1976 (u',v') values are derived for each TCS. The values (u', v') are taken as coordinates and the area that inscribes the polygon is calculated, this value is the Gamut Area. Finally the Gamut Area Index (GAI) normalizes with respect to GA of an equal Energy Spectrum Source, is shown in equation (4.12).

$$
GAI=\frac{GA}{0.00728468}100
\tag{4.12}
$$

4.3.4. CONSTRUCTION OF THE TRAINING SET

The database consists of 125496 SPD samples corresponding to the combination of different available light sources (LED, incandescent, fluorescent and Sun). That is, SPD samples containing a certain percentage of disturbance were generated in order to recreate real conditions in which more than one light source is present, and thus validate that the results are useful in the applications where the use of the model is proposed.

Each of the light sources is combined with the remaining considering 3 different disturbance ranges, with 6 values in each range. In first case the disturbance varies from 2% to 12% (e.g. 98% incandescent + 2% LED, then 96% incandescent + 4% LED, etc). In the second range the variation is from 6% to 36% and finally the disturbance varies from 8.3% to 50%. For each range, a training dataset of 41832 samples is obtained. The chosen light sources are from different manufacturers, including Osram, General Electric, Philips, and Sylvania. The measured CRI varied between 55.22 and 99.90 and the GA between 35.79 and 98.24.

The variables of the RGB sensor and 10 linear and nonlinear combinations of them, are considered as inputs for the Deep Learning stage (R,G,B,R^2,G^2,B^2,R/G,R/B,G/B,1).

4.3.5. EXPERIMENT DESCRIPTION

In Figure 4.1, the left side represents the input to the system, which will be the radiation in the visible spectrum. Composed with the combination of SPD, this radiation would be absorbed and represented (converted into electronic signals) by the RGB sensor (1). The channel data is scaled to the input of the MLP as described above (R, G, B, R^2, G^2, B^2, R/G, R/B, G/B, 1), then the trained MLP (2) calculates the value of the CRI and the GAI (3) for the SPD incident on the RGB sensor. The training process is performed in reverse, using the set described in the previous section to teach the examples to the MLP.

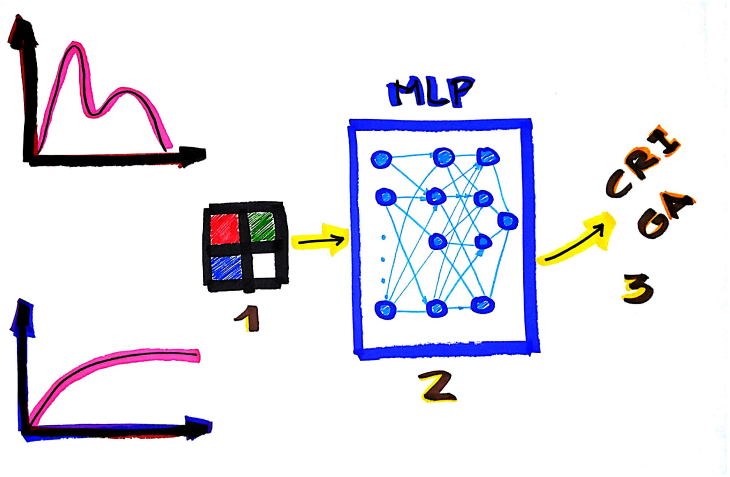

Figure 4.1 Experiment description

4.3.6. TYPES OF SOURCES USED

Figure 4.2a shows three samples of LED sources. The white LED sources are constructed by combining (overlapping) several types of LEDs, these LEDs are overlapped to obtain a white response according to the manufacturers' standards. One of the possibilities of future work, based on the results of this work, is to control a LED light source to match a polychromatic illumination system where the GAI and CRI cannot be controlled. Figure 4.2b shows three samples of fluorescent sources.

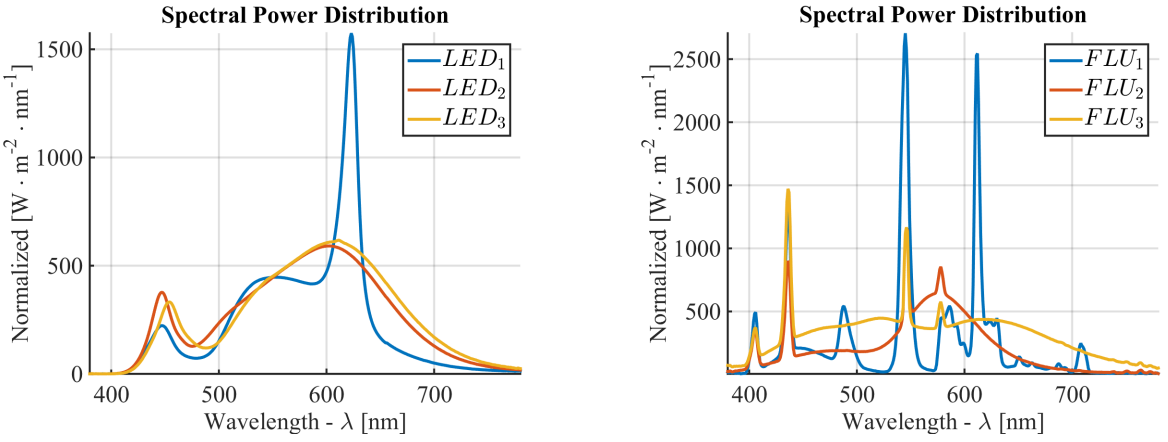

(a) SPD LED Sources

(b) SPD Fluorescent sources

Figure 4.2 SPD LED and fluorescent

In Figure 4.3a, three samples of incandescent light sources are shown. The CRI in incandescent sources is usually high, in values ranging from 93 to 99. The spectra of incandescent light sources are characterized as being soft and having a significantly high component in the infrared spectrum. The infrared part of their spectrum causes their energy inefficiency. In Figure 4.3b shows the spectrum of the Sun on three different days.

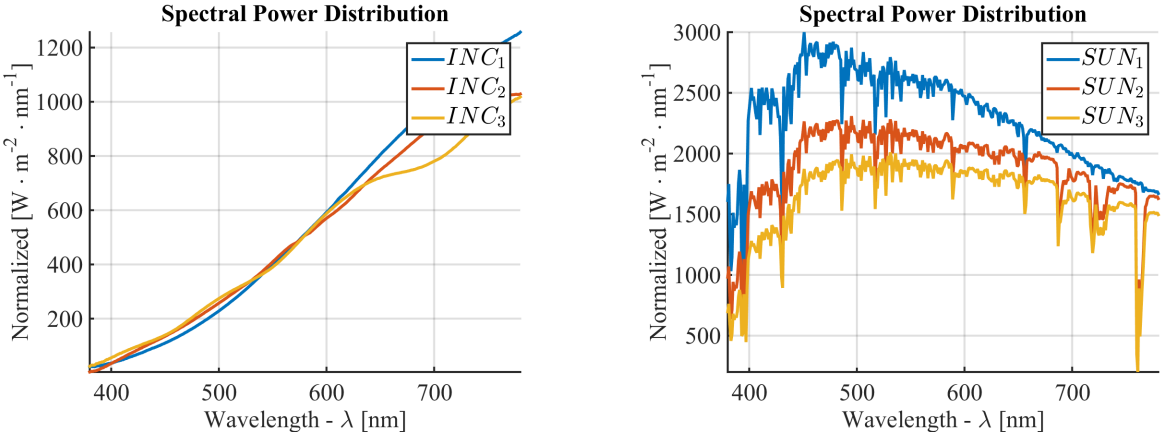

(a) SPD incandescent Sources

(b) SPD Sun source

Figure 4.3 SPD incandescent and SUN

4.4. RESULTS AND DISCUSSION

4.4.1. SPECTRAL RESPONSE OF THE SENSOR

The spectral response of the sensors was calculated employing the model described in Chapter 2, where a broadband light source, a monochromator and a high-resolution spectrometer were used in order to construct the characteristic curve, and measurements of spectra were taken every 10 nm in the range between 380 nm and 780 nm. However, in this case an interpolation method was used to know the spectral response every 1 nm instead of 10 nm. The spectral response curve of both sensors is presented in Figure 4.4.

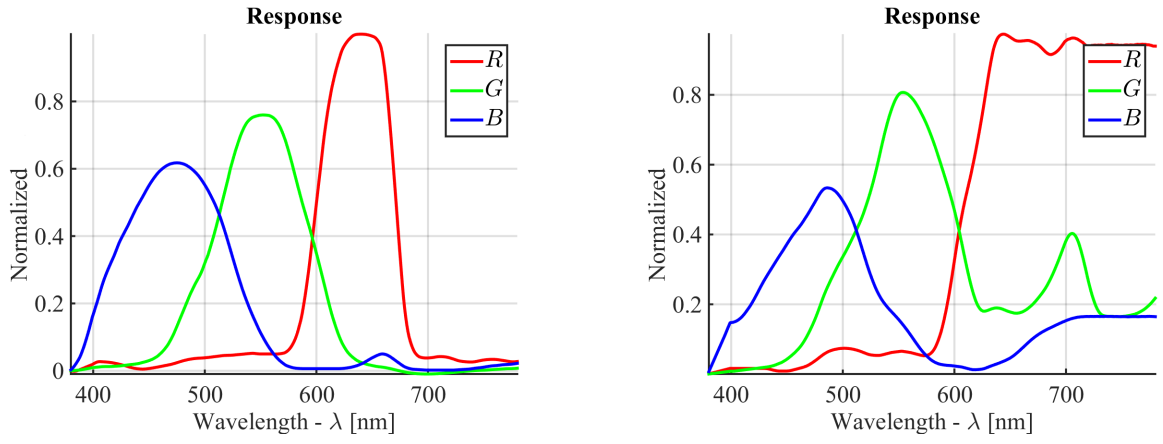

(a) Response TS3414CS

(b) Response ADJDS311

Figure 4.4 Response TS3414CS and ADJDS311

DISTRIBUTION OF TRAINING SETS

In figure 4.5, the histogram of the CCT values for the subset A and B is displayed. It can be seen that these are distributed in the sample space of the variable and therefore, there are enough examples for training.

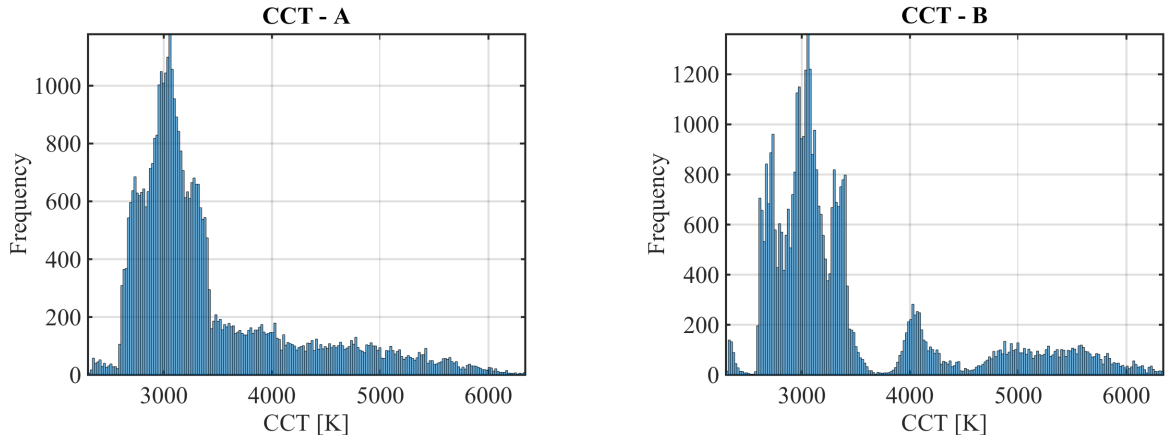

(a) CCT-A (b) CCT-B

Figure 4.5 CCT distributions

The purpose of having big datasets in the training of algorithms of automatic learning, is to sample the space of characteristics, so that the possible combinations of entrance of the system are represented in the examples. In figure 4.6, the histogram of the CRI values for the subset B and C is displayed. It can be observed that these are distributed with greater density between 80 and 100 as is expected in white light sources.

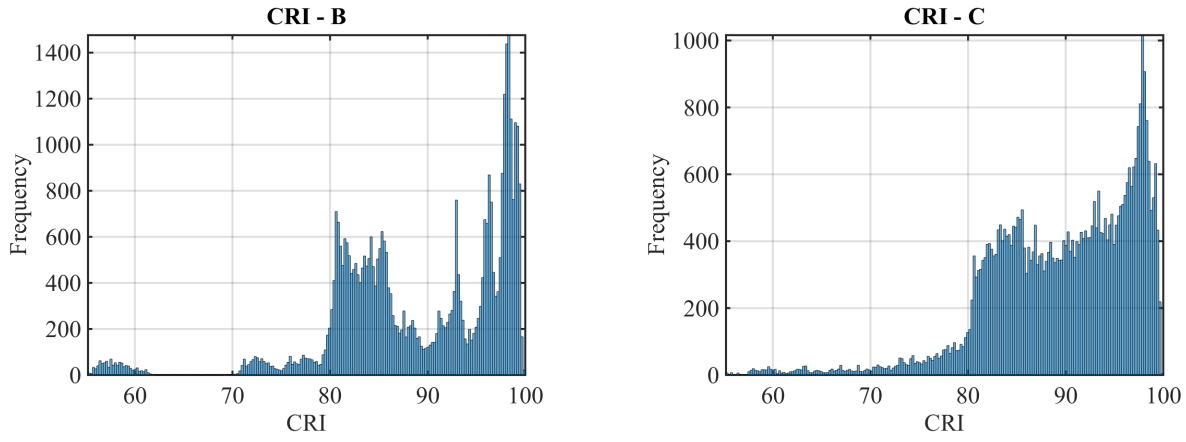

(a) CRI-B (b) CRI-C

Figure 4.6 CRI distribution

In figure 4.7, the histogram of the GAI values for the subset A and C is displayed. In the density of the Gamut Area Index, it is observed a lower concentration than in the histogram of CCT and CRI, this is more distributed in the range of the variable. The highest concentration is between 40 and 80. The GAI will be one of the variables to be estimated by the architecture proposed in this work.

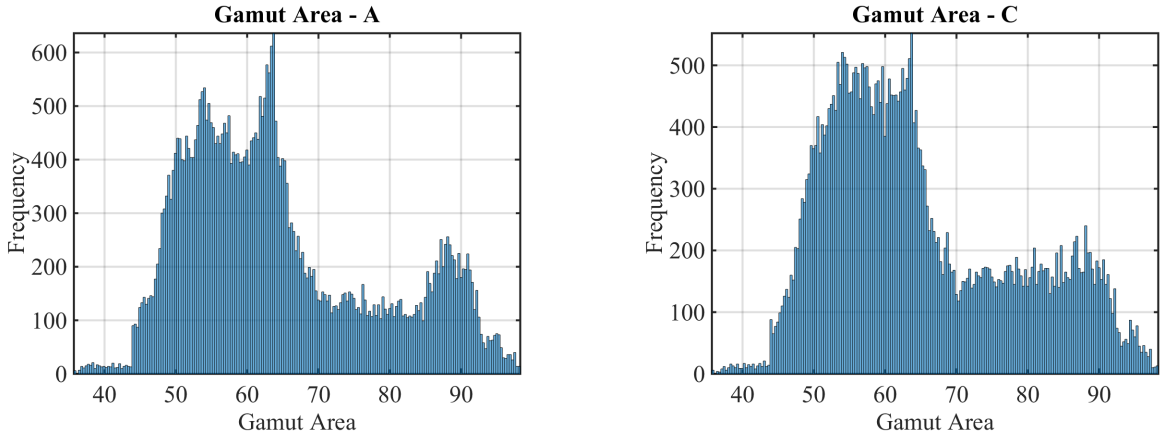

(a) GAI-A (b) GAI-C

Figure 4.7 GAI distribution

It is also important to evaluate the distribution of input information from the input training set. Figure 4.8 shows the histogram of the TCS3414CS sensor response for each of its channels (RGB) to the subset B and C, respectively.

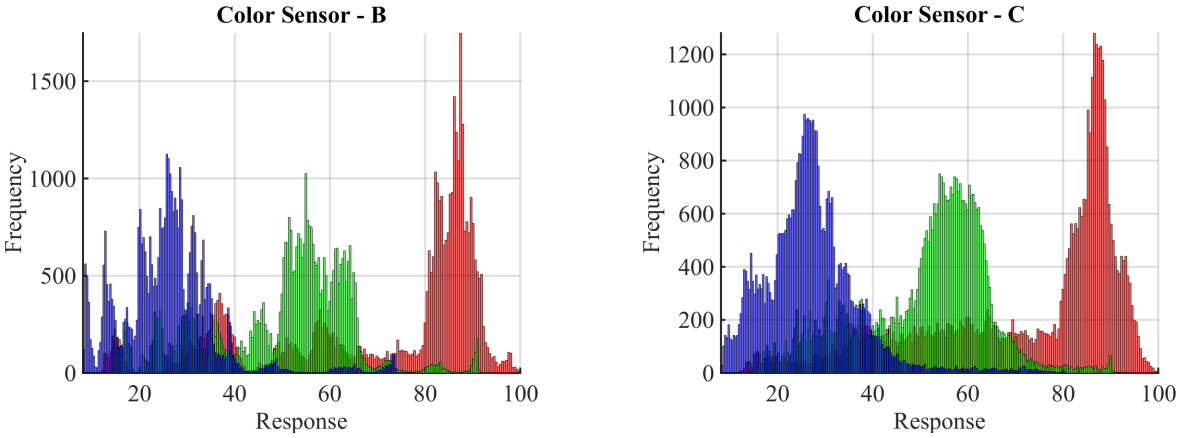

(a) TCS3414CS-B (b) TCS3414CS-C

Figure 4.8 TCS3414CS response distribution

Figure 4.9 shows the histogram of the ADJDS311 sensor response for each of its channels (RGB) to the subset B and C, respectively. It can be seen that there is a much greater overlap in the distribution between the R and B channels. Overlap could reduce the amount of information delivered by the sensor to the sources, and therefore could represent greater difficulty in convergence.

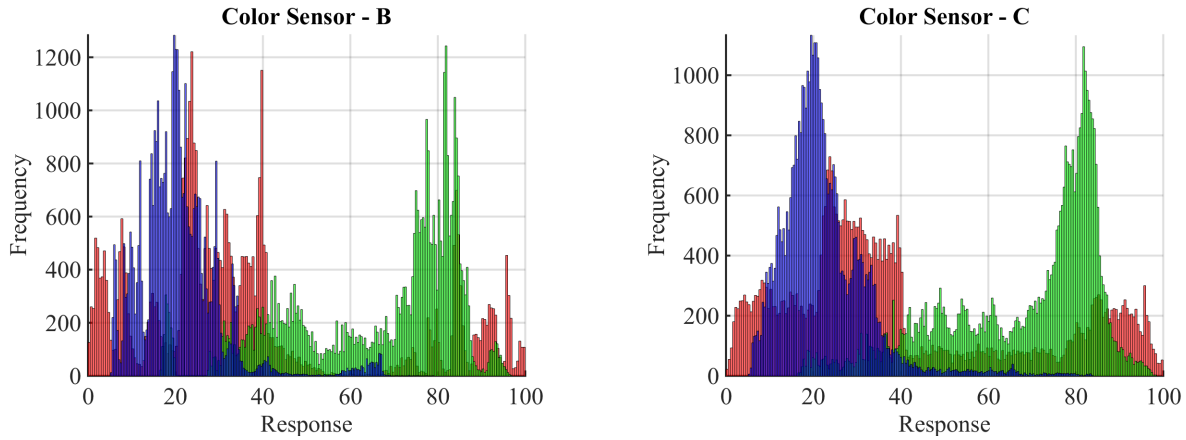

(a) ADJDS311-B (b) ADJDS311-C

Figure 4.9 ADJDS311 response distribution

4.4.2. VALIDATION ERROR

As mentioned above, the three training subsets (A, B and C) were mixed in a single set. For the training of each of the 640 architectures this set was separated into two test subsets, one of 70% (88547 examples) for training, and one of 30% (37949) for validation. Figure 4.10 shows the validation error for the calculation of the GAI and the CRI (sensor TCS3414CS) where the activation functions of the MLP were sigmoidal tangents (NL). In this case, the training was done using the resources of the CPU of the Workstation.

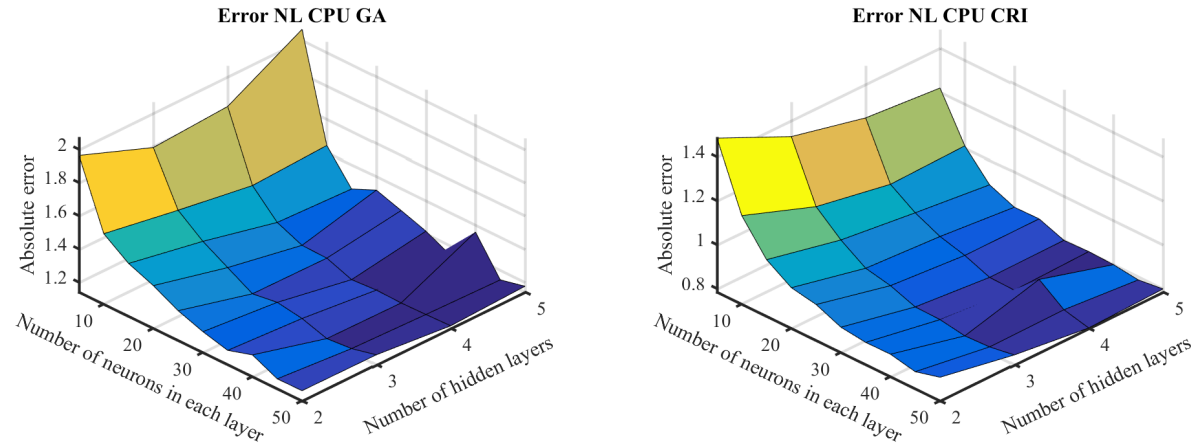

(a) Error NL CPU GA TCS3414CS (b) Error NL CPU CRI TCS3414CS

Figure 4.10 Error GA CRI TCS3414CS

Figure 4.11 shows the comparison of the training surface to estimate the CRI of the two sensors trained with GPU and CPU, respectively.

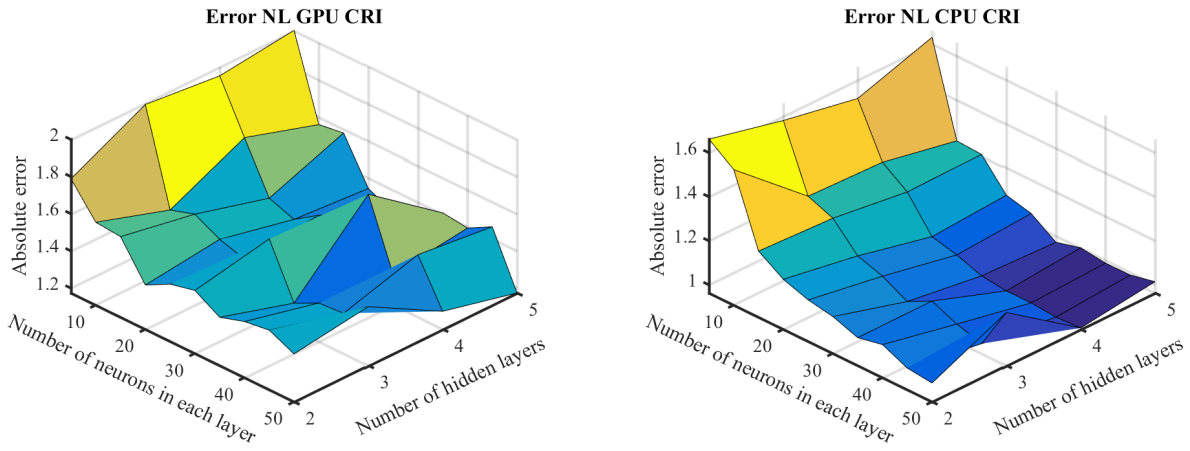

(a) Error NL GPU CRI TCS3414CS

(b) Error NL CPU CRI ADJDS311

Figure 4.11 Error CRI TC3414CS ADJDS311

Figure 4.12 shows the comparison of the training surface to estimate the CRI of the ADJDS311 sensor trained with GPU with the linear and non-linear activation function. In general, the use of the GPU reduces the processing time; however, due to the numerical representation and the loss of precision the error is usually higher as it was observed in all the trainings of the architecture developed in this work.

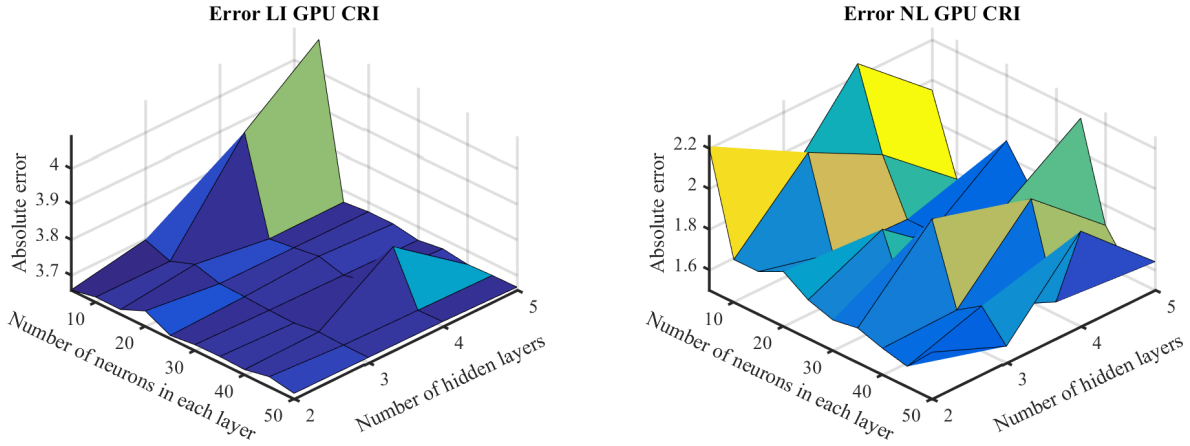

(a) Error LI GPU CRI ADJDS311

(b) Error NL GPU CRI ADJDS311

Figure 4.12 Error NL GPU CRI ADJDS311

The training with the CPU shows a better convergence (due to the use of the floating point), but, as was shown below, also implies a longer training time. In the Tables 4.3, 4.4, 4.5 and 4.6 the rows (2, 3, 4, 5) represent the number of layers and the columns (5, 10, 15, 20, ... 50) the number of neurons in each hidden layer.

The tables show the absolute validation error. In Table4.3, 4.4, 4.5 and 4.6 the error shown corresponds to the tansig function. This architecture shows the best results.

Table 4.3 Error TCS3414CS NL CPU GA

	5	**10**	**15**	**20**	**25**	**30**	**35**	**40**	**45**	**50**
2	1,96	1,57	1,46	1,40	1,32	1,27	1,23	1,27	1,20	1,20
3	1,79	1,49	1,37	1,29	1,20	1,22	1,20	1,15	1,16	1,20
4	1,82	1,42	1,27	1,20	1,20	1,14	1,15	1,15	1,15	1,16
5	2,07	1,44	1,25	1,32	1,27	1,22	1,14	1,36	1,14	1,18

Table 4.4 Error ADJDS311 NL CPU GA

	5	**10**	**15**	**20**	**25**	**30**	**35**	**40**	**45**	**50**
2	2,04	1,73	1,64	1,53	1,44	1,41	1,37	1,35	1,32	1,29
3	1,98	1,66	1,48	1,42	1,52	1,33	1,31	1,24	1,29	1,29
4	1,92	1,69	1,42	1,37	1,31	1,31	1,26	1,27	1,33	1,25
5	2,89	1,56	1,38	1,33	1,33	1,25	1,97	1,28	1,26	1,31

Table 4.5 Error TCS3414CS NL CPU CRI

	5	**10**	**15**	**20**	**25**	**30**	**35**	**40**	**45**	**50**
2	1,49	1,19	1,04	0,97	0,95	0,90	0,89	0,89	0,86	0,89
3	1,33	1,06	0,97	0,89	0,87	0,83	0,82	0,81	0,81	0,83
4	1,25	1,00	0,93	0,87	0,84	0,80	0,79	0,90	0,81	0,79
5	1,22	1,01	0,89	0,84	0,84	0,80	0,80	0,80	0,78	0,80

Table 4.6 Error ADJDS311 NL CPU CRI

	5	**10**	**15**	**20**	**25**	**30**	**35**	**40**	**45**	**50**
2	1,66	1,58	1,26	1,19	1,15	1,13	1,09	1,11	1,06	1,05
3	1,58	1,29	1,25	1,13	1,09	1,03	1,09	1,04	1,01	1,20
4	1,52	1,28	1,20	1,05	1,03	0,99	0,97	0,97	0,96	0,97
5	1,63	1,22	1,21	1,08	1,05	0,97	1,00	0,99	0,99	1,01

4.4.3. PROCESSING TIME

Finally, in the tables 4.7 and 4.8 the processing time of each architecture is shown for the calculation of each index. The rows represent the number of hidden layers (2,3,4,5). In comparison, the total processing time using only the CPU was 129: 01 hours, while with the GPU the total time was 19:22, less than 7 % of the CPU time. In both tables is highlight the architectures in which the lowest validation error was obtained.

Table 4.7 Training CPU processing time

	TCS3414CS-LI		ADJDS311-LI		TCS3414CS-NL		ADJDS311-NL	
HL	GA	CRI	GA	CRI	GA	CRI	GA	CRI
2	00:03	00:03	00:04	00:02	02:46	02:38	03:25	02:55
	3,02	2,64	3,27	3,67	1,20	0,89	1,29	1,05
3	00:08	00:08	00:09	00:08	04:40	06:06	06:52	03:19
	3,02	2,64	3,27	3,67	1,20	0,83	1,29	1,20
4	00:16	00:19	00:20	00:24	08:18	10:45	11:04	09:45
	3,02	2,64	3,27	3,67	1,16	0,79	1,25	0,97
5	00:57	00:55	01:15	00:57	10:16	18:22	10:52	10:37
	3,02	2,64	3,27	3,67	1,18	0,80	1,31	1,01
T	01:25	01:26	01:49	01:33	26:00	37:52	32:15	26:37

Table 4.8 Training GPU processing time

	TCS3414CS-LI		ADJDS311-LI		TCS3414CS-NL		ADJDS311-NL	
HL	GA	CRI	GA	CRI	GA	CRI	GA	CRI
2	00:09	00:08	00:10	00:09	00:37	00:42	00:32	00:43
	3,02	2,65	3,26	3,67	1,99	1,43	2,49	1,73
3	00:15	00:11	00:12	00:12	01:00	00:52	00:57	00:36
	3,02	2,64	3,27	3,67	2,22	1,49	1,90	1,58
4	00:25	00:25	00:16	00:17	01:11	01:15	00:44	00:42
	3,04	2,64	3,26	3,67	1,70	1,27	2,52	1,97
5	00:38	00:27	00:30	00:26	01:12	01:51	00:29	00:53
	3,02	2,64	3,26	3,67	1,65	1,17	2,42	1,64
T	01:28	01:13	01:09	01:05	04:02	04:43	02:42	02:55

4.5. CONCLUSIONS

In this paper, a methodology was proposed to estimate the CRI and the GAI using the information provided by low cost RGB sensors with a Multi-Layer Perceptron (MLP). The validation error showed the effectiveness of the methodology, the absolute error was below 2% for all cases. The architecture can be easily implemented to measure chromatic reproduction characteristics in real-time. This information is very useful for the tuning of polychromatic sources in places where external disturbances occur or to detect disturbances in color measurement processes that require controlled conditions.

As part of this work we also built a database (the training set), with mixed SPD that will allow the training of new models, or the simulation of lighting conditions.

Finally, it is important to understand that these types of estimation alternatives are developed in order to reduce the costs of measurement with respect to the use of spectrometers and to be able to perform implementations where distributed measurements (multiple points) are made on test surfaces, i.e. the measurement of chromatic reproduction characteristics is not punctual.

REFERENCES

[1] M. Ashe, D. Chwastyk, C. de Monasterio, M. Gupta, and M. Pegors, "2010 U .S. Lighting Market Characterization," Navigant Consulting, Tech. Rep. January, 2012.

[2] N. Thejokalyani and S. Dhoble, "Novel approaches for energy efficient solid state lighting by RGB organic light emitting diodes – A review," *Renewable and Sustainable Energy Reviews*, vol. 32, pp. 448–467, 2014.

[3] M. Aldrich, A. Badshah, B. Mayton, N. Zhao, and J. A. Paradiso, "Random walk and lighting control," in *2013 IEEE Sensors*. Baltimore: IEEE, 2013, pp. 1–4.

[4] M. Magno, T. Polonelli, L. Benini, and E. Popovici, "A low cost, highly scalable wireless sensor network solution to achieve smart LED light control for green buildings," *IEEE Sensors Journal*, vol. 15, no. 5, pp. 2963–2973, 2015.

[5] L. Bellia, A. Pedace, and F. Fragliasso, "Indoor lighting quality: Effects of different wall colours," *Lighting Research and Technology*, pp. 1–16, 2015.

[6] F. M. Vossen, M. P. Aarts, and M. G. Debije, "Visual performance of red luminescent solar concentrating windows in an office environment," *Energy and Buildings*, vol. 113, pp. 123–132, 2016.

[7] T. E. Kuhn, H. R. Wilson, J. Hanek, and M. Santamouris, "Raout-in: Color rendering of objects in a daylit room viewed from outdoors," *Energy and Buildings*, vol. 118, pp. 93–98, 2016.

[8] F. Gassmann, U. Krueger, T. Bergen, and F. Schmidt, "Comparison of luminous intensity distributions," *Lighting Research and Technology*, pp. 1–22, 2015.

[9] E. Palacios-Garcia, A. Chen, I. Santiago, F. Bellido-Outeiriño, J. Flores-Arias, and A. Moreno-Munoz, "Stochastic model for lighting's electricity consumption in the residential sector. Impact of energy saving actions," *Energy and Buildings*, vol. 89, pp. 245–259, 2015.

[10] R. D. Lingard, M. A. Myer, and M. L. Paget, "Performance of Incandescent A-Type and Decorative Lamps and LED Replacements," Pacific Northwest National Laboratory, Richland, Washington, Tech. Rep., 2008.

[11] M. A. Myer, M. L. Paget, and R. D. Lingard, "Performance of T12 and T8 Fluorescent Lamps and Troffers and LED Linear Replacement Lamps," Pacific Northwest National Laboratory, Richland, Washington, Tech. Rep. January, 2009.

[12] M. L. Paget, R. D. Lingard, and M. A. Myer, "Performance of Halogen Incandescent MR16 Lamps and LED Replacements," Pacific Northwest National Laboratory, Richland, Washington, Tech. Rep., 2008.

[13] F. Behar-Cohen, C. Martinsons, F. Viénot, G. Zissis, A. Barlier-Salsi, J. P. Cesarini, O. Enouf, M. Garcia, S. Picaud, and D. Attia, "Light-emitting diodes (LED) for domestic lighting: Any risks for the eye?" *Progress in Retinal and Eye Research*, vol. 30, no. 4, pp. 239–257, 2011.

[14] A. Pandharipande and D. Caicedo, "Daylight integrated illumination control of LED systems based on enhanced presence sensing," *Energy and Buildings*, vol. 43, no. 4, pp. 944–950, 2011.

[15] S. Afshari, S. Mishra, A. Julius, F. Lizarralde, J. D. Wason, and J. T. Wen, "Modeling and control of color tunable lighting systems," *Energy and Buildings*, vol. 68, pp. 242–253, 2014.

[16] J. M. Miller, Michael E.; Gilman, Jacob M.; Colombi, "A model for a two-source illuminant allowing daylight colour adjustment," *Lighting Research and Technology*, pp. 1–14, 2014.

[17] X. Feng, W. Xu, Q. Han, and S. Zhang, "Colour-enhanced light emitting diode light with high gamut area for retail lighting," *Lighting Research and Technology*, pp. 1–14, 2015.

[18] C.-w. Tang, B.-j. Huang, and S.-p. Ying, "Illumination and Color Control in Red-Green-Blue Light-Emitting Diode," *IEEE Transactions on Power Electronics*, vol. 29, no. 9, pp. 4921–4937, sep 2014.

[19] P. Bodrogi, Y. Lin, X. Xiao, D. Stojanovic, and T. Khanh, "Intercultural observer preference for perceived illumination chromaticity for different coloured object scenes," *Lighting Research and Technology*, pp. 1–11, 2015.

[20] A. Tuzikas, A. Žukauskas, R. Vaicekauskas, P. Vitta, and M. Shur, "Cultural Preferences to Color Quality of Illumination of Different Artwork Objects Revealed by a Color Rendition Engine," *IEEE Photonics Journal*, vol. 5, no. 4, pp. 6 801 010–6 801 010, 2013.

[21] P. Bodrogi, S. Brückner, T. Q. Khanh, and H. Winkler, "Visual assessment of light source color quality," *Color Research & Application*, vol. 38, no. 1, pp. 4–13, 2013.

[22] P. Bodrogi, C. Schiller, and T. Khanh, "Testing the CIE system for mesopic photometry in a threshold detection experiment," *Lighting Research and Technology*, pp. 1–13, 2015.

[23] Y. Lin, M. Wei, K. Smet, A. Tsukahara, and P. Bodrogi, "Colour preference varies with lighting application," *Lighting Research and Technology*, pp. 1–13, 2015.

[24] D. L. Loe, "Light, vision and illumination: The interaction revisited," *Lighting Research and Technology*, vol. 48, no. 2, pp. 176–189, 2016.

[25] ASSIST, "Guide to Light and Color in Retail Merchandising," Lighthing Research Center, Tech. Rep. 1, 2010. [Online]. Available: http://www.lrc.rpi.edu/programs/solidstate/assist/

[26] ——, "Recommendations for Specifying Color Properties of Light Sources for Retail Merchandising," Lighthing Research Center, Tech. Rep. 2, 2010. [Online]. Available: http://www.lrc.rpi.edu/programs/solidstate/assist/

[27] F. Szabo, R. Keri, J. Schanda, P. Csuti, A. Wilm, and E. Baur, "A study of preferred colour rendering of light sources: Shop lighting," *Lighting Research and Technology*, vol. 48, no. 3, pp. 286–306, may 2016.

[28] Y. Guo, Y. Liu, A. Oerlemans, S. Lao, S. Wu, and M. S. Lew, "Deep learning for visual understanding: A review," *Neurocomputing*, vol. 187, pp. 27–48, 2016.

[29] Y. Dong, Y. Liu, and S. Lian, "Automatic age estimation based on deep learning algorithm," *Neurocomputing*, vol. 187, pp. 4–10, apr 2016.

[30] M. Längkvist, L. Karlsson, and A. Loutfi, "A review of unsupervised feature learning and deep learning for time-series modeling," *Pattern Recognition Letters*, vol. 42, pp. 11–24, 2014.

[31] M. A. Rahhal, Y. Bazi, H. AlHichri, N. Alajlan, F. Melgani, and R. Yager, "Deep Learning Approach for Active Classification of Electrocardiogram Signals," *Information Sciences*, vol. 345, pp. 340–354, 2016.

[32] J. Leng and P. Jiang, "A deep learning approach for relationship extraction from interaction context in social manufacturing paradigm," *Knowledge-Based Systems*, vol. 100, pp. 188–199, 2016.

[33] Z. Y. Wu, M. El-Maghraby, and S. Pathak, "Applications of Deep Learning for Smart Water Networks," *Procedia Engineering*, vol. 119, pp. 479–485, 2015.

[34] E. Mocanu, P. H. Nguyen, M. Gibescu, and W. L. Kling, "Deep learning for estimating building energy consumption," *Sustainable Energy, Grids and Networks*, vol. 6, pp. 91–99, 2016.

[35] E. Mocanu, P. H. Nguyen, W. L. Kling, and M. Gibescu, "Unsupervised energy prediction in a Smart Grid context using reinforcement cross-building transfer learning," *Energy and Buildings*, vol. 116, pp. 646–655, 2016.

[36] Q. Hu, R. Zhang, and Y. Zhou, "Transfer learning for short-term wind speed prediction with deep neural networks," *Renewable Energy*, vol. 85, pp. 83–95, 2016.

[37] J. Gomes, J. Correia, and J. Carmo, "A Low-Cost Flexible-Platform (LCFP) for characterization of photodetectors," *Measurement*, vol. 61, pp. 206–215, 2015.

[38] J.-S. Botero V., F.-E. Lopez G., and J.-F. Vargas B., "Characterization of photodectors using a monochromator and a broadband light source in the XYZ color space," *International journal on Smart Sensing and Intelligent Systems*, vol. 9, no. 2, pp. 752–764, 2016. [Online]. Available: http://s2is.org/Issues/v9/n2/papers/paper18.pdf

[39] J. E. Agudo, P. J. Pardo, H. Sánchez, A. L. Pérez, and M. I. Suero, "A low-cost real color picker based on arduino." *Sensors*, vol. 14, no. 7, pp. 11 943–56, 2014.

[40] J.-S. Botero V., F.-E. Lopez G., and J.-F. Vargas B., "Calibration method for Correlated Color Temperature (CCT) measurement using RGB color sensors," in *Symposium of Signals, Images and Artificial Vision - 2013: STSIVA - 2013*. Bogotá: IEEE, 2013, pp. 1–6.

[41] ——, "Calibration Method for Measuring the Color Rendering Index (CRI) using RGB Sensor," *Tecnológicas*, vol. EE, pp. 325–338, 2013.

[42] ——, "Classification of artificial light sources and estimation of Color Rendering Index using RGB sensors , K Nearest Neighbor and Radial Basis Function," *International Journal on Smart Sensing and Intelligent Systems*, vol. 8, no. 3, pp. 1505–1524, 2015. [Online]. Available: http://www.s2is.org/Issues/v8/n3/papers/paper5.pdf

[43] J.-S. Botero V., S.-M. Navarro, N. Giraldo, and L. Atehortua, "Estimation of Photosynthetically Active Radiation (PAR) using a low cost spectrometer," *IEEE Latin America Transactions*, vol. 12, no. 2, pp. 107–111, 2014.

[44] C. S. McCamy, "Correlated color temperature as an explicit function of chromaticity coordinates," *Color Research & Application*, pp. 142–144, 1992.

5

ESTIMATION OF THE REFLECTANCE CURVE

Contents

5.1. ABSTRACT

The reflectance of objects, is the property that represents the percentage of power that is not absorbed when it is radiated with an electromagnetic wave. Its representation is essential in color measurement and studies of material properties. In Lambertian surfaces it is considered that the reflection occurs with equal magnitude in all directions, i.e. changing the point of view, does not change the luminance. That said, reflectance represents the only property of a material that can change its perception of color. Reflectance is a wavelength dependent property. For the particular case discussed in this work, and in the most common measurement method it can be used a spectrophotometer, an integrating sphere and a white light source to determine it. However, this involves high costs and additionally a punctual measurement. For this reason, this work presents a method to measure reflectance on a flat surface using an array of LEDs a monochromatic camera and a power control system. The results show that an error of less than 22% for the worst case and less than 9% for 87% of the samples can be reached. This work is aimed at developing methods to estimate the reflectance of flat Lambertian surfaces, which are inexpensive and allow a distributed measurement on the surface, i.e. it can be estimated in regions of pixels.

5.2. INTRODUCTION

The reflectance represents the percentage of power that is not absorbed by an object when it is radiated with an electromagnetic wave. In most materials the reflectance changes with the wavelength and for this reason, its value is expressed as a function. Its representation is fundamental for the measurement of color and for studying material properties. In Lambertian surfaces it is considered that the reflection occurs with equal magnitude in all directions, that is, when changing the point of view, the reflectance value does not change. The study of measurement models of reflectance is relevant due to the wide field of applications in the analysis and characterization of materials [1–6], and in the measurement of color, when multispectral sources are used in the visible spectrum with a principle directly related to the reflectance function [7–11]. The idea of using LED lighting as an active element for measuring color has been widely developed [12–16]. In [16], for example, one of the simplest approximations is presented. In this, an LED and a photo-diode are used to determine the color of a surface considering its reflectance; the method is novel and really economical, however, it only can differentiate between 8 colors. In [15], a low cost system is presented that uses RGB LED as active element for the analysis of mixtures of five common food dyes. In this case the analysis process is based on the estimation of the absorbance of the mixtures; similar work had been previously developed [17, 18]. Currently, more complex systems have been implemented, in which multispectral sources are constructed using LED illumination [10, 19–21] in order to measure color. Many of these focus only on the final implementation (color), and base the selection of bands on human perception criteria, and although the final implementation can be reduced, material information can be sacrificed; and this is one of the reasons why this work focuses on the reflectance function, without ignoring, but without distinguishing a particular application. Given their versatility and spectral stability, LEDs have also been used to reconstruct other illuminants (reconstruct specific spectra) [22, 23] and to develop applications in medicine [24] where the source is used to improve perception. In [23], a work is presented where a hyperspectral source is developed that operates between 400 and 700 nm with 31 bands. Its purpose is to rebuild standard illuminants. The results are good and show another possible application for the source developed in our work that although it has only 23 bands, is of greater power, which allows a better resolution with low-cost detectors and large area samples.

In this work, we present a method that uses a monochromatic camera and a group-controlled high power LED array with 23 bands to measure reflectance on a flat surface. The method was tested with a 24-patch Color Checker Passport. The results show that an error of less than 22% can be reached in the worst case and less than 9% for 87% of the samples. Additionally, calibration methods have been developed, which will be useful in other applications. The aim of this work is to develop methods to estimate the reflectance of flat Lambertian surfaces, which are inexpensive and allow distributed measuremenst on the surface to perform color measurements or material characterization.

5.3. MATERIALS AND METHODS

5.3.1. LED SOURCE

The most important element in this chapter, is the selection and characterization of the hyperspectral LED source. For this, initially, LEDs were selected and characterized by the market, and later they were searched with specialized suppliers, in such a way that they help to cover the visible spectrum in the best way while maintaining a low cost. It is important to clarify that part of the contribution of the method presented in this work is to prove that the estimation can be done without a uniform distribution (in wavelength), which usually represents a high cost even in LEDs. The spectra of the 23 types of LEDs used in this work are shown in 5.1, are low-cost, commercially available, individually characterized and selected, all are $3W$ (power consumed) And it was necessary to use an external current control system in order to maintain a uniform emission power. Additionally the LED array must be coupled to a dissipation and cooling system to maintain wavelength stability.

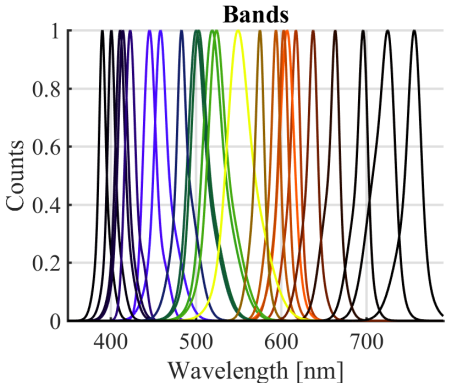

Figure 5.1 SPD LED hyperspectral source

In figure, 5.2, the x, y coordinates of the LEDs in the CIE 1931 color space are shown with black dots. It can be seen that a good mapping of the region is made, the values in the space margin represent the LEDs that are associated with only one of the human photopical responses (observer curves), the other points are those representing overlapping combinations in at least two of three the observer's curves.

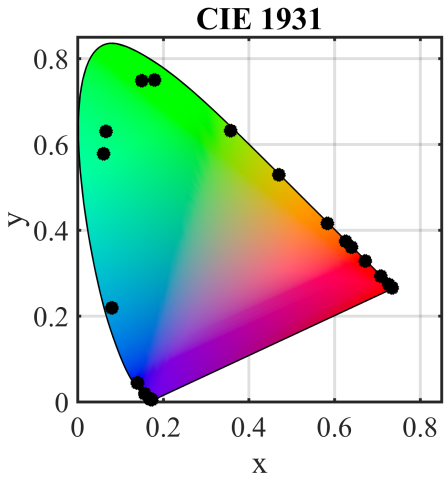

Figure 5.2 CIE 1931 - LED

In table 5.1 the values characterized for each type of LED are presented. As previously was mentioned, 23 LED types were used, the WL FAB column represents the wavelength defined by the manufacturer, the WL MES column, the wavelength measured in the laboratory under stable conditions, BW measured bandwidth, E power, V the barrier voltage and I the control current to maintain the emission of all the uniform bands. In the table 5.1 values are highlighted where the difference between the manufacturer wavelength and the measurement were distant. Since the bandwidths are variable, the total area was considered, not just the emission peak to calculate the reflectance at each point.

Table 5.1 LED characterization

WL FAB [nm]	WL MES [nm]	BW [nm]	E [J]	V [V]	I [A]
385.00	390.7	10.2	5.0843E-19	3.2	0.32
395.00	401.2	11.1	4.9513E-19	3.1	0.32
405.00	411.5	13.6	4.8273E-19	3.0	0.33
410.00	414.7	14.3	4.7901E-19	3.0	0.33
425.00	423.3	14.4	4.6928E-19	2.9	0.34
445.00	445.9	17.7	4.4549E-19	2.8	0.36
465.00	458.7	18.8	4.3306E-19	2.7	0.37
480.00	483.4	15.8	4.1093E-19	2.6	0.39
497.50	500.6	25.3	3.9681E-19	2.5	0.40
505.00	503.5	24.1	3.9453E-19	2.5	0.41
522.50	519.3	28.8	3.8252E-19	2.4	0.42
530.00	524.3	26.7	3.7888E-19	2.4	0.42
550.00	549.6	35.2	3.6143E-19	2.3	0.44
570.00	575.3	13.2	3.4529E-19	2.2	0.46
591.00	594.0	13.3	3.3442E-19	2.1	0.48
627.50	603.1	13.9	3.2937E-19	2.1	0.49
602.50	607.0	20.6	3.2726E-19	2.0	0.49
597.50	617.4	14.2	3.2174E-19	2.0	0.50
640.00	637.6	14.1	3.1155E-19	1.9	0.51
660.00	663.4	14.5	2.9943E-19	1.9	0.54
700.00	696.1	15.2	2.8537E-19	1.8	0.56
730.00	724.9	27.6	2.7403E-19	1.7	0.58
760.00	756.0	20.7	2.6276E-19	1.6	0.61

5.3.2. COLOR CHECKER

The color checker is a color palette with 24 samples arranged in 4 rows. The reflectance of the samples are known, allowing to use it as a reference standard. In figure 5.3 the distribution of the colors is shown, correspond to a photo of the color checker used in this work.

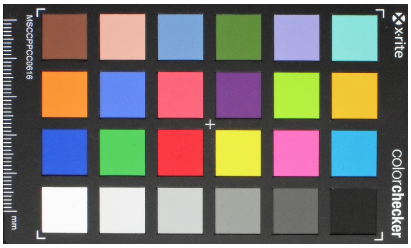

Figure 5.3 Color Checker Passport

5.3.3. EXPERIMENT DESCRIPTION

In Figure 5.4 the explanatory diagram of the proposed experiment is presented and its parts are described below:

1. Initially a capture in total dark of the detector is realized to know the dark noise and the necessary corrections are applied to validate the quality and operation of the camera (uniformity and bad pixels)

2. Then, 23 matrices were built each of 6 LED's where each matrix contains LED's with the same wavelength or its variation is less than 4 nm, they can be identified in (2)

3. A monochroatic camera is located in the center of the LED array and is connected via USB to a desktop computer (4). The camera parameters are controlled manually and are kept static for all the captures of the experiment

4. At the base of the system, at 0.35 m from the camera, the Color Checker is placed in order to occupy the area of vision and the radiation emitted by the LEDs is enough so that when reflected, it is detected by the pixels of the camera

5. The LED's for each wavelength. The purpose is to adjust the power so that the reading in static conditions of the camera for the white patch is 254 in digital value, ie, the patch with higher reflectance is about to saturate the photodetector. This process is automatic, the patch is previously segmented to be measured and to vary the response of the controller (3).

6. After balancing the power in the previous number, 5 frames are acquired for each wavelength, stored and labeled, in each frame not saturation at the sensor is verified

7. Finally, an arithmetic average of the 5 frames corresponding to each wavelength is made, then the 24 patches are segmented in each averaged frame, and 8 points of each patch are taken. This digital value corresponds to the reflectance ratio of the respective patch, to the reflectance of the white patch (254 in digital) at the wavelength of the frame, with this information the reflectance curves are reconstructed

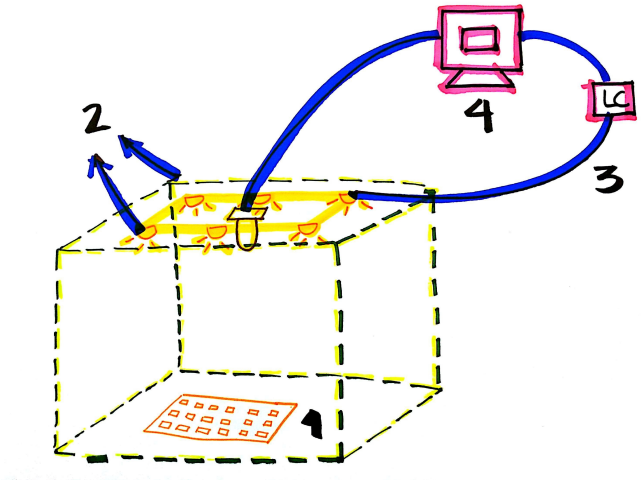

Figure 5.4 Experiment description

5.4. RESULTS AND DISCUSSIONS

In Figure 5.5, 23 images acquired with the monochromatic camera FL3-U3-13Y3M-C are shown after being adjusted with the target response and convoluted with a media filter. Each image corresponds to the response when the Color Checker is illuminated by a particular LED type (specific wavelength Table 5.1). The images show changes due to the reflectance that each patch has at the wavelength with which it is radiated, the purpose is to be able to obtain reflection values for the 24 patches in a single image. Additionally, an automatic segmentation algorithm was developed that allows the process of separation of the patches.

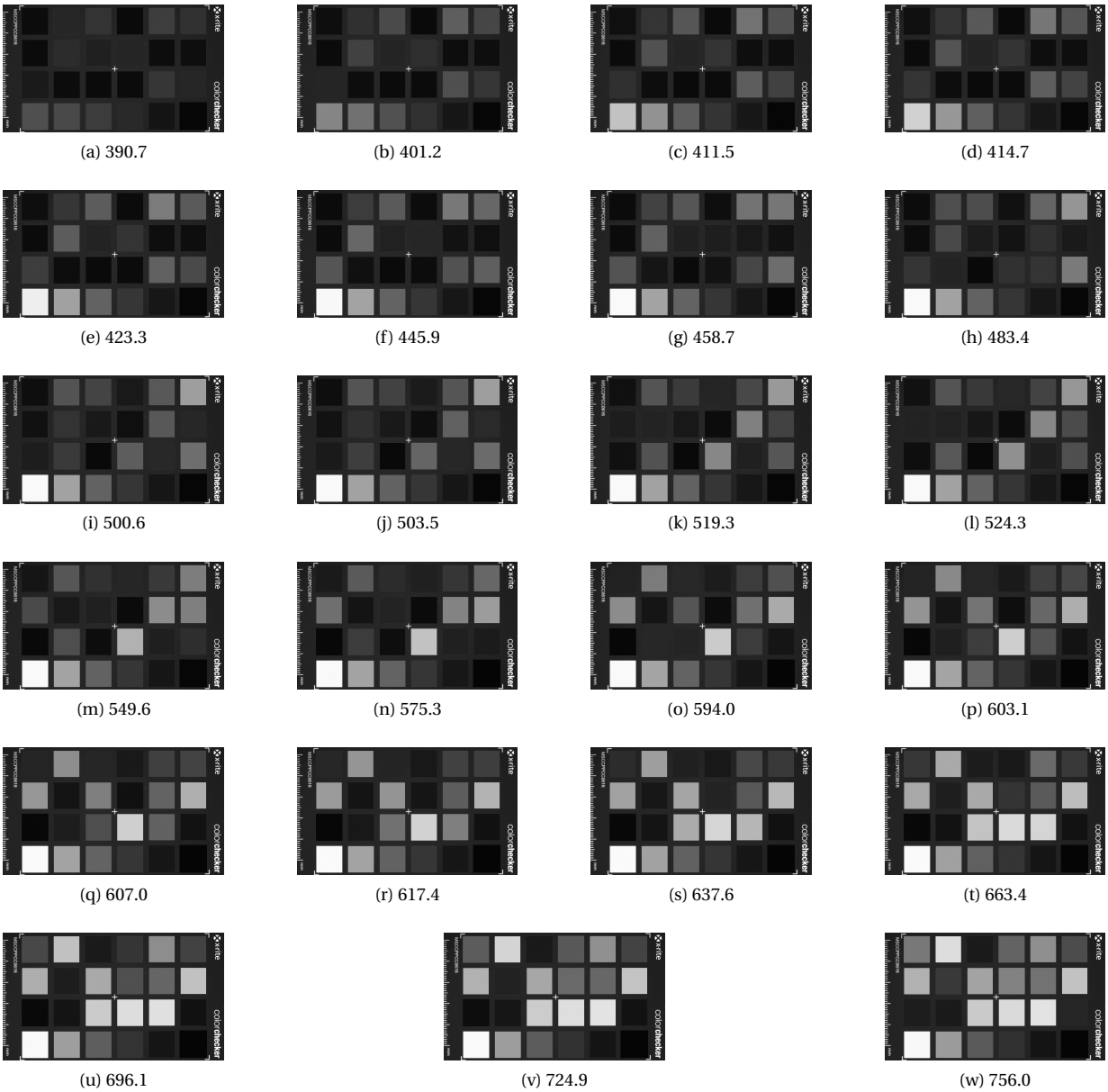

(a) 390.7 (b) 401.2 (c) 411.5 (d) 414.7

(e) 423.3 (f) 445.9 (g) 458.7 (h) 483.4

(i) 500.6 (j) 503.5 (k) 519.3 (l) 524.3

(m) 549.6 (n) 575.3 (o) 594.0 (p) 603.1

(q) 607.0 (r) 617.4 (s) 637.6 (t) 663.4

(u) 696.1 (v) 724.9 (w) 756.0

Figure 5.5 Color Checker images

In figure 5.6 the measured reflectances for each of the 24 patches are shown in blue and the estimated reflectances are shown in red, in the original matrix distribution but in the vertical position, P1 corresponds to the patch brown and P24 to the black. The X axis is the wavelength and the Y axis the normalized reflectance, the units are omitted to avoid reloading the figure.

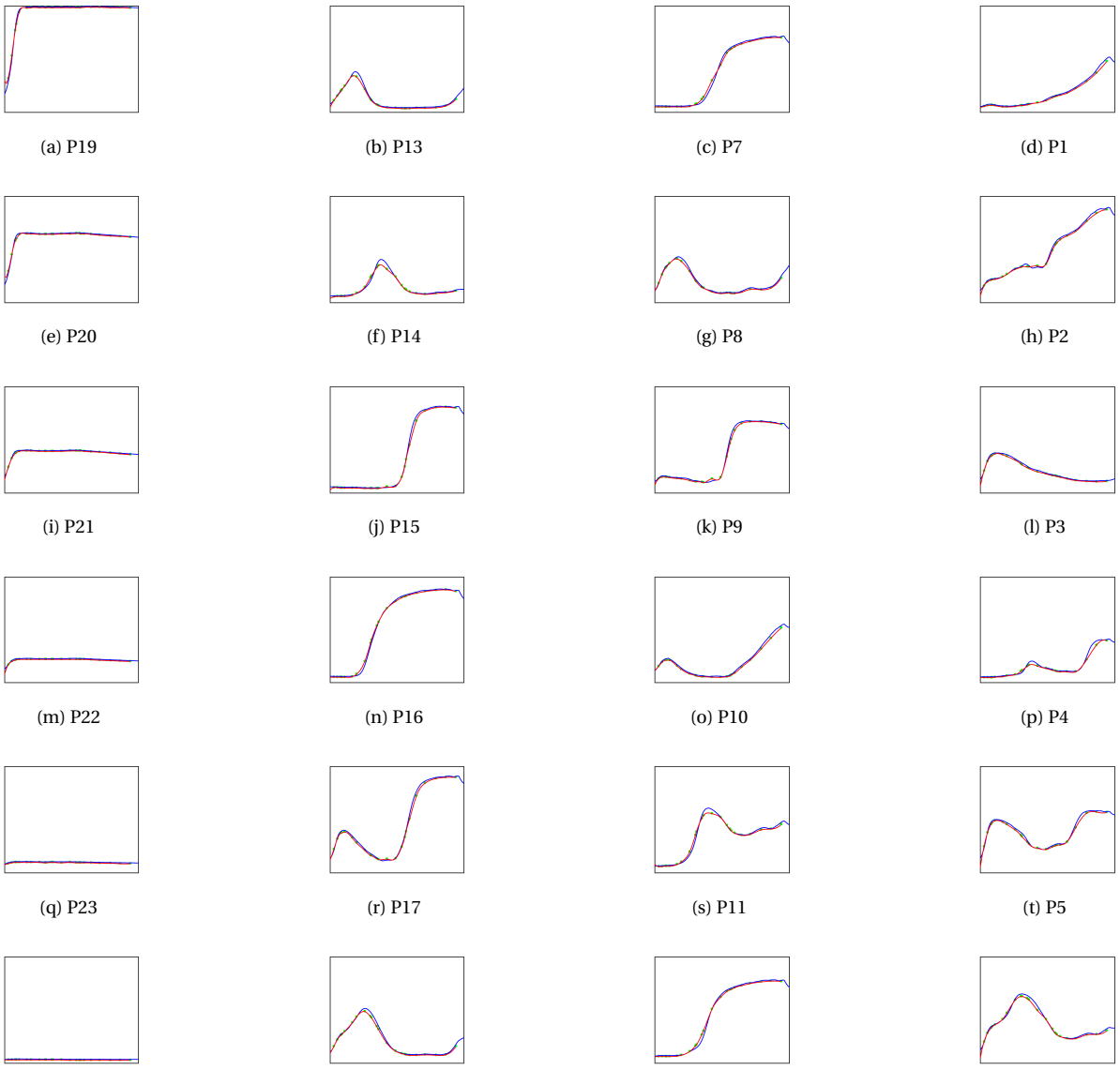

(a) P19 (b) P13 (c) P7 (d) P1

(e) P20 (f) P14 (g) P8 (h) P2

(i) P21 (j) P15 (k) P9 (l) P3

(m) P22 (n) P16 (o) P10 (p) P4

(q) P23 (r) P17 (s) P11 (t) P5

(u) P24 (v) P18 (w) P12 (x) P6

Figure 5.6 Color Checker reflectance estimation

Finally, in Table 5.2, the absolute reflectance estimation error is presented for each one of 24 Color Checker patch curves. The Table has the standard Color Checker distribution, (R1, C1) is the brown and (R4, C6) is the black. It can be observed that the greatest error occurs in the black curve, due to its low reflectance and the proximity to the minimum response threshold of the photodetector. It can also be observed that in 21 patches the error is less than 9% which can be considered an acceptable response if the cost of implementation is taken into account. The manufacturer does not offer specific reflectance curves but they are widely disseminated in the literature and for the development of this work they were measured with a spectrometer.

Table 5.2 Error reflectance estimation

	C1	C2	C3	C4	C5	C6
R1	0.0813	0.0343	0.0555	0.0894	0.0437	0.0400
R2	0.0870	0.0643	0.0508	0.0911	0.0580	0.0562
R3	0.1288	0.0810	0.0856	0.0652	0.0427	0.0653
R4	0.0254	0.0215	0.0214	0.0418	0.0802	0.2270

5.5. CONCLUSIONS

In this work a method was proposed that allows to estimate the reflectance of a flat surface using a hyperespectral LED source of 23 bands that are not uniformity spaced. The results showed that the error is less than 9% for 21 patches of a Color Checker Passport and that it is acceptable as a low cost estimation method.

Since the presented method allows to estimate the spectral reflectance curve of the surface, it is possible, from this one, to calculate the color perception of the same with different sources, this is one of the main purposes of this work, aimed at reducing costs in the measurement of color and to have information that allows to simulate the perception of surfaces to different sources of light.

In future implementations of the method, it is planned to construct the LED array in such a way as to allow spatial availability of all LEDs so that the group switching procedure is not manual and the procedure can be performed in a shorter time, not implemented in this work because the availability of LED cooling cells was limited.

Another interesting variable to observe in future work is the relationship between the spectral location of the LEDs and the error, ie, some regions have a higher density of LED bands and an error threshold could be defined that would be used to reduce the number of bands, reducing the cost of implementation and the acquisition time for a particular implementation.

REFERENCES

[1] F. H. Imai, R. S. Berns, and D.-Y. Tzeng, "A Comparative Analysis of Spectral Reflectance Estimated in Various Spaces Using a Trichromatic Camera System," *Journal of Imaging Science and Technology*, vol. 44, no. 4, pp. 280–287, 2000.

[2] A. Ghauch, C. Turnar, C. Fachinger, J. Rima, A. Charef, J. Suptil, and M. Martin-Bouyer, "Use of diffuse reflectance spectrometry in spot test reactions for quantitative determination of cations in water," *Chemosphere*, vol. 40, no. 12, pp. 1327–1333, 2000.

[3] S. Y. El-Zaiat, "Determination of the complex refractive index of a thick slab material from its spectral reflectance and transmittance at normal incidence," *Optik - International Journal for Light and Electron Optics*, vol. 124, no. 2, pp. 157–161, 2013.

[4] S. Kotthaus, T. E. Smith, M. J. Wooster, and C. Grimmond, "Derivation of an urban materials spectral library through emittance and reflectance spectroscopy," *ISPRS Journal of Photogrammetry and Remote Sensing*, vol. 94, pp. 194–212, aug 2014.

[5] N. Xie, H. Wang, and D. Feng, "Coating materials to increase pavement surface reflectance," in *Eco-Efficient Materials for Mitigating Building Cooling Needs*. Elsevier, 2015, pp. 13–35.

[6] A. Fernández-García, F. Sutter, L. Martínez-Arcos, C. Sansom, F. Wolfertstetter, and C. Delord, "Equipment and methods for measuring reflectance of concentrating solar reflector materials," *Solar Energy Materials and Solar Cells*, vol. 167, pp. 28–52, aug 2017.

[7] J. Pospíšil, J. Hrdý, and J. Hrdý, "Basic methods for measuring the reflectance color of iron oxides," *Optik - International Journal for Light and Electron Optics*, vol. 118, no. 6, pp. 278–288, 2007.

[8] F. A. Saeed and J. R. G. Evans, "Measurement of diffuse reflectance from combinatorial samples," *Analytica chimica acta*, vol. 677, no. 1, pp. 79–89, 2010.

[9] M. Parmar, S. Lansel, and J. Farrell, "An LED-based lighting system for acquiring multispectral scenes," in *Proc. SPIE 8299, Digital Photography VIII*, vol. 8299, Burlingame, California, 2012, pp. 1–8.

[10] R. Shrestha, J. Y. Hardeberg, and C. Boust, "LED Based Multispectral Film Scanner for Accurate Color Imaging," *2012 Eighth International Conference on Signal Image Technology and Internet Based Systems*, pp. 811–817, 2012.

[11] C. Godau, M. Klammer, T. Eckhard, M. Schnitzlein, D. Nowack, B. Frei, and P. Urban, "Evaluation of a multispectral camera system for inline color measurement," *Annual meeting of the German Colour Group*, 2013. [Online]. Available: http://www.idd.tu-darmstadt.de/media/fachgebiet{_}idd/forschungdienstleistung/color/publikationen{_}6/GODAU{_}FWS13.pdf

[12] J. Laming and A. Martino, "PC color recognition using LED and software techniques," *IEEE Photonics Technology Letters*, vol. 5, no. 5, pp. 583–586, may 1993.

[13] F. A. Matias, M. M. Vila, and M. Tubino, "A simple device for quantitative colorimetric diffuse reflectance measurements," *Sensors and Actuators B: Chemical*, vol. 88, no. 1, pp. 60–66, 2003.

[14] Ö. G. Saracoglu and H. Altural, "Color Regeneration from Reflective Color Sensor Using an Artificial Intelligent Technique," *Sensors (Basel, Switzerland)*, vol. 10, no. 9, pp. 8363–8374, sep 2010.

[15] M.-H. Sorouraddin, A. Rostami, and M. Saadati, "A simple and portable multi-colour light emitting diode based photocolourimeter for the analysis of mixtures of five common food dyes," *Food Chemistry*, vol. 127, no. 1, pp. 308–313, jul 2011.

[16] M. Assaad, I. Yohannes, A. Bermak, D. Ginhac, and F. Meriaudeau, "Design and characterization of automated color sensor system," *International journal on smart sensing and intelligent systems*, vol. 7, no. 1, pp. 1–12, 2014. [Online]. Available: http://s2is.org/Issues/v7/n1/papers/paper1.pdf

[17] K.-T. Lau, W. S. Yerazunis, R. L. Shepherd, and D. Diamond, "Quantitative colorimetric analysis of dye mixtures using an optical photometer based on LED array," *Sensors and Actuators B: Chemical*, vol. 114, no. 2, pp. 819–825, apr 2006.

[18] M.-H. Sorouraddin and M. Saadati, "A simple fabrication of portable diffuse reflectometer for simultaneous analysis of common food dyes," *Sensors and Actuators B: Chemical*, vol. 145, no. 1, pp. 367–372, 2010.

[19] J.-I. Park, M.-H. Lee, M. D. Grossberg, and S. K. Nayar, "Multispectral Imaging Using Multiplexed Illumination," *2007 IEEE 11th International Conference on Computer Vision*, pp. 1–8, 2007.

[20] R. Shrestha and J. Y. Hardeberg, "Multispectral imaging using LED illumination and an RGB camera," in *21st Color and Imaging Conference Final Program and Proceedings*, 2013, pp. 8–13. [Online]. Available: http://english.hig.no/content/download/42793/638549/file/Shrestha-CIC2013.pdf

[21] A. M. Peter, "Design and Evaluation of LED Illumination Source for Multispectral Imaging Applications," Ph.D. dissertation, Cochin University of Science and Technology, 2015.

[22] K. Yuan, H. Yan, and S. Jin, "LED-based spectrally tunable light source with optimized f itting," *Chin. Opt. Lett.*, vol. 12, no. 3, p. 32301, 2014. [Online]. Available: http://col.osa.org/abstract.cfm?URI=col-12-3-032301

[23] F. J. Burgos, M. Vilaseca, E. Perales, J. A. Herrera-Ramírez, F. M. Martínez-Verdú, and J. Pujol, "Spectral LED-Based Tuneable Light Source for the Reconstruction of CIE Standard Illuminants," in *Lecture Notes in Computer Science*. Springer International Publishing, 2014, pp. 115–123.

[24] P. Bartczak, A. Gebejes, P. Falt, and M. Hauta-Kasari, "An LED-Based Tunable Illumination for Diverse Medical Applications," *2016 IEEE 29th International Symposium on Computer-Based Medical Systems (CBMS)*, pp. 292–293, 2016.

6

MODEL INTEGRATION

Contents

6.1. ABSTRACT

Color measurement is a fundamental process for the development of all industries where the quality control is performed on the appearance of the same. As explained in the course of this manuscript, the color is dependent on light and the reflection function, however, the standardized form of measurement requires widely controlled conditions that complicate its implementation or require expensive equipment for this purpose. For this reason, in this manuscript methods were presented to obtain the sensitivity of photodetectors, monochromatic cameras, derived photometric measurements from RGB sensors and to obtain the reflectance function with a hyperspectral LED source. All these methods are oriented to the training of an MLP, which can estimate the XYZ value of a sample, even though it is exposed to an external disturbance, ie in the process of reflectance estimation, the sample is exposed to the known hyperspectral source and to external sources, too, that the MLP is able to compensate. The compensation is achieved by the low-cost RGB sensor, which estimates the CRI and GAI of the disturbing source in the test space. The results show that the estimation error is below 1% for all cases and that the error reduces to less than half in the MLP, with the help of the photometric indices. It is important to note that the results of the feasibility of a low-cost color measurement system that could operate autonomously with an error under a single external disturbance.

6.2. MATERIALS AND METHODS

6.2.1. EXPERIMENT DESCRIPTION

In Figure 6.2 the explanatory diagram of the proposed experiment is presented and its parts are described below:

1. Initially, the characteristics of the camera are adjusted with the procedure described in 3. In addition to this, with the process of guaranteeing or knowing the number of defective pixels, the regions where they are, the level of uniformity and that the sensitivity of the camera adjusts to the manufacturer's description.

2. The test surface is marked as (1); it is in the field of the monochromatic camera (5) and the hyperspectral LED source (2). The reflectance function is obtained using the method described in the chapter 5. This function delivers the reflectance value after being adjusted for each of the 23 previously described bands, which feeds the MLP that estimates the color in the XYZ space. Figure 6.1 show example of reflectance points and interpolation for 19 patch in Color Checker.

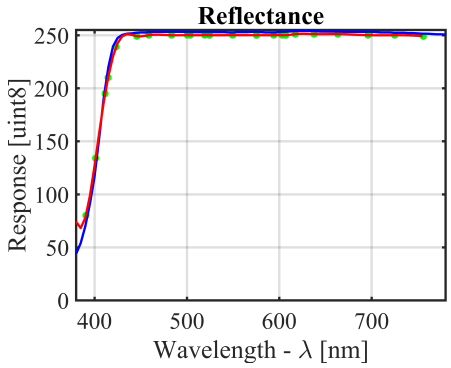

Figure 6.1 Architecture of the implementation

3. In the experiment (6) a previously calibrated low-cost RGB sensor (chapter 2) is shown, which obtains the light that disturbs the test surface and converts the information into CRI and GAI indices, as explained in chapter 4. The purpose is to feed the MLP that performs the estimation of the XYZ space.

4. Finally, (8) is the MLP that collects the reflectance information (23 bands) and the estimated CRI and GAI from the RGB sensor. The output of (8) is the color estimate in the XYZ space.

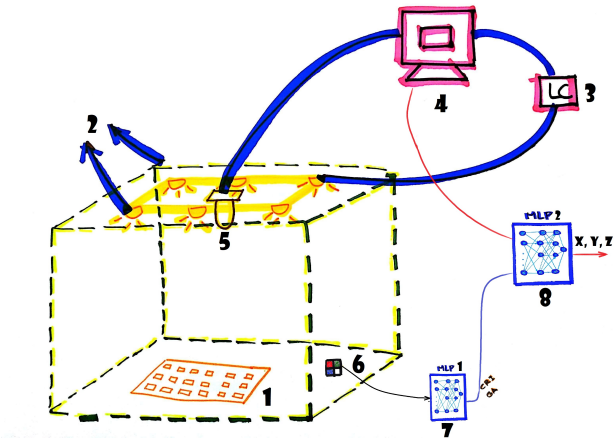

Figure 6.2 Architecture of the implementation

6.2.2. CONSTRUCTION OF THE TRAINING SET

Given the need to feed the MLP with a high training set to perform the training and validation of the proposed method, and that the error of the previous phases is known experimentally, an artificial set was constructed for the MLP training of the experiment described in Figure 6.2 (8). For this we considered several elements. The 41832 sources of the set A were used as perturbations. Reflectance functions were estimated from the ColorChecker functions. Each patch was combined with all patches, ie 24x24 reflectance functions were obtained. Each reflectance function was disturbed with 200 different sources, randomly selected from the set of 41832 sources, previously described. A training set was constructed with 115,200 samples, where the reflectance functions are represented by the error associated with the external light source disturbance. The CRI and GAI value associated with the disturbance and the actual XYZ value for each sample. With this information the MLP that is presented as final result in this work was trained.

6.3. RESULTS AND DISCUSSION

6.3.1. MODEL VALIDATION ERROR

In Figure 6.3 we see the training curve for the MLP and the output X (color space value). For the training, we used two different input sets: Input 1, where the input of the MLP are the 23 reflectance values and, additionally, the values of CRI and GAI, and Input 2, where the values of CRI and GAI are not taken into account. In addition, 2-layer and 3-layer MLPs were trained, as well as the number of neurons in each layer was varied between 3 and 18 for each of the XYZ channels. In total, 72 different architectures were trained. It was noticed that the error is lower due to the use of the indices, which implies that they contribute significant knowledge to the system.

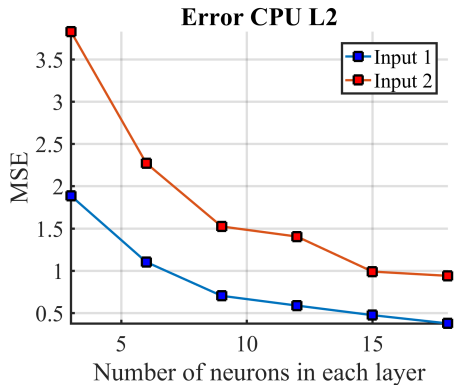

(a) 2 Hidden layers X

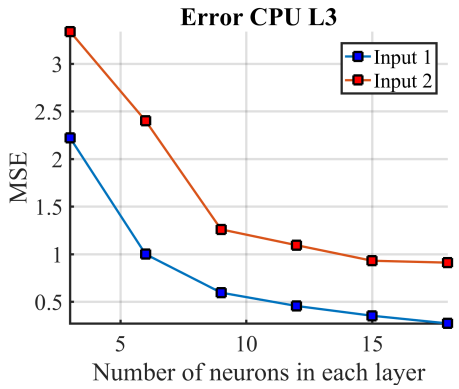

(b) 3 Hidden layers X

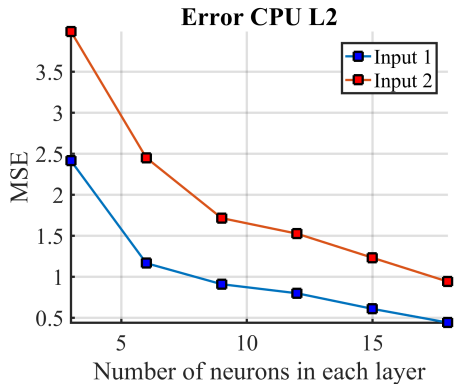

(c) 2 Hidden layers Y

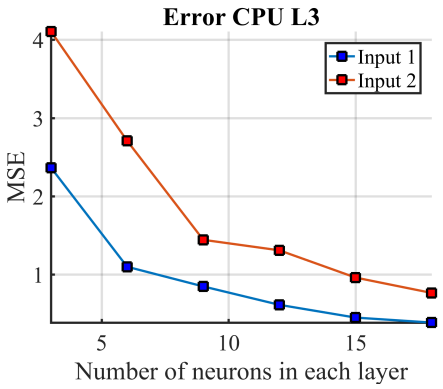

(d) 3 Hidden layers Y

Figure 6.3 Estimation Error X, Y

In Figure 6.3, the error for the Y channel is observed, again the improvement in the performance because of the use of the photometric indices is evident. It is important to clarify that this error comes from the validation and is obtained with 30% of the samples of the training set, ie with 34 560 samples. Finally, in Figure 6.4 the error for the Z channel is shown. The trend remains the same. The error of the MLP trained with Input 1 is always less than half of the error of the MLP trained with Input 2.

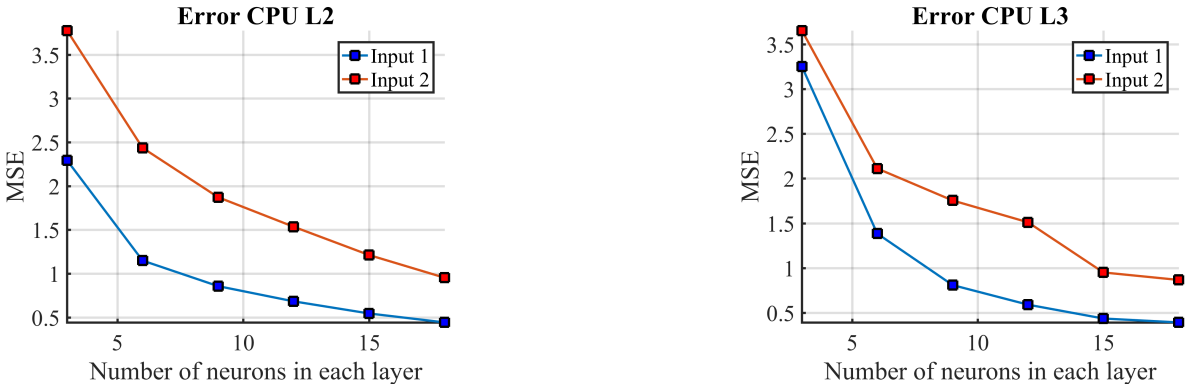

(a) 2 Hidden layers

(b) 3 Hidden layers

Figure 6.4 Estimation Error Z

In Table 6.1 the estimation error for each of the 72 architectures trained in this chapter is summarized. It can be observed that the error using the photometric indices (CRI and GAI) is always lower, which means that they provide information to the system, and that in the end the system presents robustness to external perturbations in its main purpose of obtaining the standardized XYZ values of the surface.

Table 6.1 Trainning error XYZ estimation

			H3	H6	H9	H12	H15	H18
X	Input 1	L2	1.8862	1.1026	0.7028	0.5872	0.4741	0.3764
		L3	2.2221	0.9991	0.5948	0.4547	0.3521	0.2715
	Input 2	L2	3.8287	2.2707	1.5231	1.4035	0.9894	0.9392
		L3	3.3387	2.4011	1.2597	1.0933	0.9301	0.9102
Y	Input 1	L2	2.4137	1.1634	0.9065	0.7961	0.6062	0.4385
		L3	2.3655	1.0998	0.8484	0.6133	0.4504	0.3867
	Input 2	L2	3.9905	2.4493	1.7131	1.5232	1.2298	0.9385
		L3	4.1061	2.7091	1.4439	1.3097	0.9617	0.7653
Z	Input 1	L2	2.2943	1.1489	0.8571	0.6831	0.5446	0.4425
		L3	3.2513	1.3844	0.8091	0.5902	0.4355	0.3921
	Input 2	L2	3.7762	2.4362	1.8726	1.5353	1.2119	0.9528
		L3	3.6535	2.1118	1.7545	1.5106	0.9503	0.8666

6.3.2. PAPER SAMPLES

Additionally, comparative tests were carried out with a sample of paper previously characterized and sampled with a commercial colorimeter. Figure 6.5 shows the 8 available samples. The value measured by the colorimeter was made with the standard of the observer of 2 and a source $D50$.

Figure 6.5 Paper samples

Table 6.2 show the error of estimation of the methodology proposed in this thesis. In table 6.2, XS, YZ and ZS is the color of reference, XM1, YM1 and ZM1 color measured with halogen perturbation, XM2, YM2 and ZM2 color measured with LED perturbation. As it is observed the error is always lower than 0.03, the scale of the space XYZ is normalized to 1.

Table 6.2 Measurement error

	XS	YS	ZS	XM1	YM1	ZM1	XM2	YM2	ZM2	EX1	EX2	EY1	EY2	EZ1
Red	0.38	0.23	0.1	0.36	0.21	0.08	0.35	0.20	0.09	0.02	0.03	0.02	0.03	0.02
Purple	0.45	0.42	0.66	0.46	0.41	0.64	0.43	0.40	0.63	-0.01	0.02	0.01	0.02	0.02
Yellow	0.69	0.74	0.24	0.72	0.72	0.23	0.66	0.71	0.22	-0.03	0.03	0.02	0.03	0.01
Pink	0.48	0.34	0.42	0.51	0.31	0.40	0.45	0.31	0.40	-0.03	0.03	0.03	0.03	0.02
Blue	0.25	0.32	0.67	0.28	0.29	0.64	0.22	0.30	0.65	-0.03	0.03	0.03	0.02	0.03
Skin	0.62	0.53	0.42	0.63	0.50	0.39	0.60	0.51	0.39	-0.01	0.02	0.03	0.02	0.03
Green	0.29	0.42	0.15	0.32	0.39	0.13	0.26	0.40	0.14	-0.03	0.03	0.03	0.02	0.02
White	0.85	0.89	1	0.88	0.87	0.97	0.82	0.86	0.99	-0.03	0.03	0.02	0.03	0.03

6.4. CONCLUSIONS

It was presented in this chapter that it is possible to develop a method for estimating the color value in the XYZ space of a sample with an error lower than 1% even though the surface is exposed to external perturbations.

It was also shown that the mixture of methods and estimators allow to reduce the estimation error and since all the tools used are low-cost, the proposed implementation would have industrial feasibility adjusting some construction parameters.

In future work, it is proposed to make adjustments on the training with a larger set of samples, subject to the availability of computer resources, to compare the final result of different architectures and evaluate the over-adjustment on them.